

# Thermodynamic growth of sea ice: assessing the role of salinity using a quasi-static modelling framework

David W. Rees Jones<sup>†</sup>

School of Mathematics and Statistics, University of St Andrews, North Haugh, St Andrews, KY16 9SS, UK

(Received 6 September 2024; revised 30 October 2024; accepted 4 December 2024)

Sea ice is a mushy layer, a porous material whose properties depend on the relative proportions of solid and liquid. The growth of sea ice is governed by heat transfer through the ice together with appropriate boundary conditions at the interfaces with the atmosphere and ocean. The salinity of sea ice has a major effect on its thermal properties so might naïvely be expected to have a major effect on its growth rate. However, previous studies observed a low sensitivity throughout the winter growth season. The goal of this study is to identify the controlling physical mechanisms that explain this observation. We develop a simplified quasi-static framework by applying a similarity transformation to the underlying heat equation and neglecting the explicit time dependence. We find three key processes controlling the sensitivity of growth rate to salinity. First, the trade-off between thermal conductivity and (latent) heat capacity leads to low sensitivity to salinity even at moderately high salinity and brine volume fraction. Second, the feedback on the temperature profile reduces the sensitivity relative to models that assume a linear profile, such as zero-layer Semtner models. Third, thicker ice has the opposite sensitivity of growth rate to salinity compared with thinner ice, sensitivities that counteract each other as the ice grows. Beyond its use in diagnosing these sensitivities, we show that the quasi-static approach offers a valuable sea-ice model of intermediate complexity between zero-layer Semtner models and full partial-differential-equation-based models such as Maykut–Untersteiner/Bitz–Lipscomb and mushy-layer models.

**Key words:** sea ice, solidification/melting

<sup>†</sup> Email address for correspondence: [david.reesjones@st-andrews.ac.uk](mailto:david.reesjones@st-andrews.ac.uk)

## 1. Introduction

Sea ice is a fundamental part of the climate of the polar regions. Sea ice evolves as it is transported by wind and ocean currents, due to various mechanical processes such as ridging, and due to thermodynamic processes of growth and melting (Golden *et al.* 2020). This study focuses on the thermodynamic aspects of the evolution.

The first goal of this study is to understand the effect of salinity on sea-ice growth through the winter growth season and to compare different representations of this process in active use in the sea-ice modelling community (these include zero-layer Semtner, Maykut–Untersteiner/Bitz–Lipscomb and dynamic-salinity mushy-layer models). The second goal is to propose a new type of quasi-static (QS) approximate model of an intermediate complexity between a zero-layer model (based on ordinary differential equations (ODEs)) and the other types of models which are all based on partial differential equations (PDEs).

The classic early work on sea-ice growth was developed by Stefan in the late nineteenth century (Stefan 1891). Historical reviews of Stefan's contribution are given by Vuik (1993) and Šarler (1995). Stefan investigated solidification problems with a free boundary between the solid and liquid phases, a class of problems subsequently called *Stefan problems*. Stefan introduced several approaches that will guide this study. The growth of ice is governed by a heat equation. Stefan applied a similarity-solution method to solve this equation analytically and also obtained approximate solutions under the assumption of a linear temperature profile. In either case, the ice thickness increases with the square root of time. This theoretical prediction was consistent with measurements of sea-ice thickness from polar expeditions.

Stefan treated sea ice as a pure material with constant thermal properties. However, sea ice forms from seawater, an aqueous solution of water and salt (of various types). The salt retained in sea ice allows pockets of saltwater (brine) to remain as liquid inclusions within a matrix of solid ice even when the composite is cooled beneath the freezing point of seawater. This part-solid and part-liquid composite is called a mushy layer. Huppert & Worster (1985) and Worster (1986) extended the similarity solution for a pure material to the solidification of a two-component (binary) alloy. A two-component alloy is a simple model of saltwater (amongst many other chemical systems). As for the pure system, the solidification front advances with the square root of time. In this study, we develop a new QS approximation. This approximation reduces to the similarity-solution method under certain conditions and so represents an extension of this body of earlier work as well as Stefan's original application of the idea.

Kerr *et al.* (1989, 1990) extended these earlier models to account for the variation of the thermal properties within the mushy layer and for variation in the bulk composition within the mushy layer. These papers parameterised heat transfer through the liquid as a turbulent heat flux rather than assuming that all the heat transfer was conductive. These extensions are important for modelling sea-ice growth because the thermal properties vary considerably and also because the heat transfer from the ocean is dominantly through turbulent convection rather than conduction. The resulting equations were solved numerically. However, the treatment was still limited because it was not known how to calculate the evolution of the bulk composition (salinity) within the mush. In practice, sea ice is observed to desalinate rapidly through a process called convective desalination driven by a compositional buoyancy gradient within the ice (see reviews by Worster 1997, 2000; Anderson & Guba 2020).

Within the sea-ice literature, Maykut & Untersteiner (1969, 1971) developed a significant new type of model (see references therein for some antecedent developments).

We refer to this model by the acronym MU. There are some similarities with the developments in mushy-layer theory outlined above (which all came later), particularly in terms of the role of salinity in the thermal properties of the ice. The MU model has the same limitation as the mushy-layer models mentioned so far in terms of having to prescribe the salinity. There are also differences. In particular, the ice is topped by a layer of snow, radiative heating is included and a realistic energy balance with the atmosphere is used. The MU model is of particular importance because it is still widely used in large-scale climate simulations, particularly in the version developed further by Bitz & Lipscomb (1999). Bitz & Lipscomb (1999) updated the MU model by accounting for the latent heat of melting the upper surface of the ice, which is important for modelling the summer melt season. However, for the winter growth season, this difference is not important since there is limited melting at that interface in winter.

The thermodynamics within the sea ice itself in the MU model is structurally entirely consistent with that used in mushy-layer theory (Feltham *et al.* 2006). Indeed, by a suitable choice of the parameter values, they can be made identical. However, the parameters used by default in MU models have a stronger sensitivity to salinity than would be suggested by mushy-layer theory (in which the thermal conductivity is a weighted average of the solid and liquid conductivity). We return to this issue later when considering suitable parameter values.

Another widely used class of sea-ice models was developed by Semtner (1976). These models use the same thermodynamic framework as the MU model, but rather than solving the full heat equation, the equation is vertically discretised into three layers (one snow layer and two sea-ice layers), with the temperature field assumed linear between the midpoints of each layer. In an appendix, Semtner (1976) proposed an even simpler ‘zero-layer’ model, in which the heat equation is not solved at all and the temperature field varies linearly across the ice. As mentioned above, this type of linear approximation was first used by Stefan (1891). We discuss why such approximations continue to work well even when the thermal properties vary strongly across the ice.

Recently, a new generation of dynamic-salinity mushy-layer models has been developed (Griewank & Notz 2013; Turner, Hunke & Bitz 2013; Rees Jones & Worster 2014; Griewank & Notz 2015). These applied theoretical developments within mushy-layer theory to calculate the evolution of bulk salinity either using a semi-analytical theory (Rees Jones & Worster 2013*a,b*) or two-dimensional numerical simulations (Wells, Wettlaufer & Orszag 2011, 2013). The particular implementation of Turner *et al.* (2013) has been implemented in large-scale models as discussed below. However, the three dynamic salinity models are all rather similar from a theoretical point of view (Worster & Rees Jones 2015). Laboratory experiments of the very early stages of ice growth by Thomas *et al.* (2020) suggest that dynamic-salinity mushy-layer models can successfully capture the initial desalination of sea ice and perform better than other types of parameterisation.

Indeed, collectively the zero-layer, MU and dynamic-salinity mushy-layer models represent the three options available to users of the CICE/Icepack software packages (Hunke *et al.* 2024*a,b*). These packages are widely used sea-ice models for large-scale simulations. A recent inter-comparison of CMIP6 models shows that these three models of sea-ice thermodynamics remain in use, with the Bitz–Lipscomb version of the MU model being the most common (Keen *et al.* 2021). One goal of our study is to understand better the differences between such models. This is motivated in part by numerical calculations in Griewank & Notz (2013) and Rees Jones & Worster (2014) that suggested introducing a dynamic salinity field had only a small effect on the ice growth. Similar results had previously been obtained with different prescribed salinity profiles by Vancoppenolle,

Fichefet & Bitz (2005). These observations are somewhat curious given the large variation in thermal properties through sea ice and how strongly these depend on salinity. In this study, we provide detailed physical reasons for this observation and show that it continues to hold across a wide range of sea-ice salinities (from ice that is almost as salty as seawater to ice that is completely desalinated).

Our study also contributes a new QS approximate model of sea ice which has an intermediate complexity between zero-layer models and PDE-based models (such as MU-type and mushy-layer models). Under constant boundary conditions, this model reduces to the similarity-solution method mentioned previously and gives an exact solution to MU-type models. Under variable boundary conditions, the solution is only approximate and so we investigate the validity of the approximation on theoretical grounds and through numerical calculation. While our study focuses on terrestrial sea ice, this type of intermediate complexity approach may be attractive for emerging research into the postulated mushy layers on icy moons (e.g. Buffo *et al.* 2020, 2021; Vance *et al.* 2021).

The structure of the paper is as follows. In § 2, we develop governing equations, non-dimensionalise them, discuss appropriate parameter values, and develop the QS approximation. In § 3, we analyse the initial growth rate of sea ice using theoretical (asymptotic) analysis and numerical calculation. We explain why salinity has a very weak effect on the growth rate. We compare our calculations with those based on zero-layer and MU-type models. In § 4, we consider the subsequent growth rate, which diminishes as the ice grows and the ocean heat flux becomes more important. We calculate the evolution of ice thickness and develop an approximate analytical solution. We return to the question of the role of salinity on ice growth. In § 5, we consider various kinds of variable conditions, particularly time-dependent atmospheric temperature and time-dependent sea-ice salinity. Then we test the validity of the QS approximation by comparing it against numerical solutions of a full PDE-based model. Finally, in § 6, we summarise our findings from the viewpoint of the implications for large-scale sea-ice modelling.

## 2. Model of sea-ice growth and the QS approximation

Sea ice is formed from seawater and consists of solid ice (the *solid phase*) and liquid saltwater/brine (the *liquid phase*). The composite will be referred to as *sea ice*, or *ice* for brevity.

The thermodynamic growth of ice is a predominantly one-dimensional process in which ice grows in the vertical  $z$  direction, where  $z$  increases downwards. The top of the ice (at the boundary with the atmosphere) lies at  $z = 0$  and the bottom (at the boundary with the ocean) lies at  $z = h$ , where  $h$  is the ice thickness. The thickness evolves in time  $t$  so  $h = h(t)$ . The primary model output is the growth rate  $\dot{h}(t)$  and, hence, by integrating in time, the thickness  $h(t)$ .

A key simplifying assumption in our model is that we treat the bulk salinity  $S$  as constant. Correspondingly, we neglect the effect of brine advection through the pores, which is the primary mechanism behind salinity evolution. As discussed in § 1, salinity evolution is an important process. However, we wish to understand why the salinity only has a small effect on ice growth, so it is simpler to have a single constant characterising the salinity. In Appendix A, we show that both the direct advective transport of heat by brine advection and the latent heat changes associated with changes in bulk salinity can be self-consistently neglected. Moreover, taking the bulk salinity as constant satisfies local salt conservation in the absence of advection and diffusion (equation (4) in Rees Jones & Worster 2014). It also satisfies global salt conservation: there is a salt flux proportional

to the ice growth rate and the difference in bulk salinity across the ice–ocean interface (equation (18) in Rees Jones & Worster 2014). While the more complete descriptions of salinity evolution described in § 1 are more realistic; nevertheless, assuming constant salinity does satisfy local and global salt conservation. Thus, we can safely analyse the temperature evolution while holding the salinity constant.

### 2.1. Temperature equation within the ice

The growth rate of ice depends on thermal transfer through the ice governed by conservation of heat within the ice,

$$\bar{c} \frac{\partial T}{\partial t} = \frac{\partial}{\partial z} \left( \bar{k} \frac{\partial T}{\partial z} \right) - L \frac{\partial X}{\partial t}, \quad (2.1)$$

where  $T(z, t)$  is the temperature and  $X(z, t)$  is the liquid (brine) fraction. The remaining quantities are the thermal properties:  $L$  is the volumetric latent heat,  $\bar{c}$  is the volumetric heat capacity and  $\bar{k}$  is the thermal conductivity. The properties  $\bar{c}$  and  $\bar{k}$  depend on the relative fraction of the ice that is occupied by solid and liquid. Weighting these properties volumetrically,

$$\bar{k} = k_l X + k_s (1 - X) \equiv k_s [1 - X \Delta k], \quad (2.2a)$$

$$\bar{c} = c_l X + c_s (1 - X) \equiv c_s [1 - X \Delta c], \quad (2.2b)$$

where a subscript  $s$  denotes a property of the solid phase and  $l$  denotes a property of the liquid phase. For the final equivalences, we define

$$\Delta k = (k_s - k_l)/k_s, \quad (2.3a)$$

$$\Delta c = (c_s - c_l)/c_s. \quad (2.3b)$$

These are dimensionless measures of the differences between the thermal properties of solid and liquid phases.

The liquid fraction depends on the temperature of the ice as well as its bulk salinity  $S$ , i.e. the weighted average of the salinity of the solid phase (which is assumed to be zero) and that of the liquid phase  $C$ . These are related by

$$S = CX. \quad (2.4)$$

We assume that phase change occurs until the system reaches a local thermodynamic equilibrium in which the liquid phase lies at the temperature-dependent freezing point. Thus,

$$C = -T/m, \quad (2.5)$$

where  $m$  is the slope of the freezing point (assumed constant). Hence, by combining with (2.4), we determine the liquid fraction

$$X = \frac{mS}{-T}, \quad (2.6)$$

and by the chain rule

$$\frac{\partial X}{\partial t} = X \frac{1}{-T} \frac{\partial T}{\partial t}. \quad (2.7)$$

Equation (2.7) allows the latent heat term on the right-hand side of (2.1) to be rewritten as an enhanced heat capacity. In particular, we write

$$c \frac{\partial T}{\partial t} = \kappa_s \frac{\partial}{\partial z} \left( k \frac{\partial T}{\partial z} \right), \quad (2.8)$$

where  $\kappa_s = k_s/c_s$  is the thermal diffusivity of the solid phase and

$$k = 1 - X\Delta k, \quad (2.9a)$$

$$c = 1 - X\Delta c + \frac{L}{c_s(-T)}X, \quad (2.9b)$$

are the dimensionless thermal conductivity and heat capacity respectively. These quantities depend on  $T$ , so (2.8) is a nonlinear diffusion equation.

## 2.2. Boundary conditions

In general, suitable boundary conditions for sea-ice evolution require the conservation of heat and salt across the interfaces. Here, we take a simplified approach.

We assume that the top of the ice is held at some temperature  $T_B$ , the atmospheric temperature. In principle, this temperature could vary in time, in which case  $T_B$  would denote the mean (time-averaged) or initial atmospheric temperature. In mushy-layer models, such a fixed temperature boundary condition is commonly used and corresponds physically to a perfectly conducting boundary. In sea-ice models, an energy flux balance is usually used. Hitchen & Wells (2016) showed that such flux balance models can be linearised and expressed as a Robin-type boundary condition involving both  $T$  and  $\partial T/\partial z$ ; such boundary conditions could be handled within our modelling framework.

We assume that the bottom of the ice is at the freezing point of seawater  $T_0 = -mS_0$ , where  $S_0$  is the salinity of seawater. This introduces a natural temperature scale to the problem

$$\Delta T \equiv T_0 - T_B, \quad (2.10)$$

which will be positive for ice growth.

Although (2.8) is a second-order equation and we already have two boundary conditions, we need an extra boundary condition to determine the evolution of the free boundary  $h(t)$ . Its evolution is determined by a generalised Stefan condition (Kerr *et al.* 1989, 1990). This condition represents the balance of heat fluxes across a narrow boundary layer below the ice–ocean interface

$$\dot{h} [c_l(T_l - T_0) + L(1 - X)_{z=h^-}] + F_T = k_s \left( k \frac{\partial T}{\partial z} \right)_{z=h^-}, \quad (2.11)$$

where  $T_l > T_0$  is the temperature of the upper ocean (assumed constant) and  $F_T$  is the turbulent heat flux supplied by the ocean. In general, the left-hand side of (2.11) is dominated by the latent heat term, but we retain the sensible heat term  $c_l(T_l - T_0)$  as it regularises the boundary condition when the liquid fraction at the interface  $X_{z=h^-} = 1$ .

We introduce a scale for the bulk salinity of sea ice relative to the salinity of the ocean

$$\hat{S} = S/S_0, \quad (2.12)$$

which will lie between 0 and 1 depending on how much the sea ice has desalinated (we discuss the range of  $\hat{S}$  in § 2.4). Note that  $X_{z=h^-} = \hat{S}$ , so  $\hat{S}$  can also be thought of as a scale for the liquid fraction.

### 2.3. Non-dimensionalisation

The growth of ice appears to have no natural length scale. Previous studies of growth in the laboratory have typically used the depth of the tank as a scale (e.g. Kerr *et al.* 1990). However, if we are interested in the long-term growth of ice, it makes more sense to use the following scale:

$$h_{\infty} = k_s \frac{\Delta T}{F_T}, \quad (2.13)$$

which is a scale estimate for the steady-state ice thickness based on estimating the steady-state balance in (2.11). It is important to note that this is a scale estimate, not the actual steady-state thickness. This scale is chosen because we want to investigate how ice growth depends on salinity, so it is convenient to non-dimensionalise with respect to a scale that does not depend on salinity. We report the actual steady-state thickness of the model in § 2.6.

Thus, we introduce a rescaled height ( $\hat{h}$ ) as well as a rescaled time ( $\tau$ ) and distance ( $\zeta$ ) coordinate system:

$$\hat{h} \equiv \frac{h}{h_{\infty}}, \quad \tau \equiv \frac{t \kappa_s}{h_{\infty}^2}, \quad \zeta \equiv \frac{z}{h_{\infty} \hat{h}}. \quad (2.14a-c)$$

The scaling for time is based on thermal diffusion across the steady-state ice thickness. The scaled temperature of ice can be written

$$\theta = \frac{T - T_B}{\Delta T}, \quad (2.15)$$

such that  $\theta$  runs between 0 and 1 from the upper (atmospheric) to the lower (oceanic) interface. We denote the scaled cold atmospheric temperature

$$\theta_B = \frac{-T_B}{\Delta T}, \quad (2.16)$$

which is greater than 1 by the definition of  $\Delta T$ . The effective scaled temperature difference across the ice–ocean boundary layer is

$$\theta_e = \frac{c_l (T_l - T_0)}{L}, \quad (2.17)$$

where we non-dimensionalise with respect to latent heat because this ratio controls the relative importance of sensible to latent heat fluxes in (2.11).

The Stefan condition (2.11) can be rescaled

$$\hat{h} \frac{d\hat{h}}{d\tau} = \frac{1}{\hat{L}} q, \quad (2.18)$$

where the scaled latent heat  $\hat{L} = L/(c_s \Delta T)$  is often called the Stefan number, and the growth rate factor  $q$  is defined by

$$q = \frac{k \frac{\partial \theta}{\partial \zeta} \Big|_{\zeta=1^-} - \hat{h}}{1 - \hat{S} + \theta_e}. \quad (2.19)$$

Thus,

$$\frac{d}{d\tau} \left( \frac{\hat{h}^2 \hat{L}}{2} \right) = q, \quad (2.20)$$



so determining  $q$  tells us how fast the square of ice thickness changes. We will often refer to  $q$ , which is the crucial output of our calculations, as the growth rate factor.

Similarly, the temperature equation (2.8) can be written in scaled form

$$c\hat{h}^2 \frac{\partial \theta}{\partial \tau} - \frac{c\zeta q}{\hat{L}} \frac{\partial \theta}{\partial \zeta} = \frac{\partial}{\partial \zeta} \left( k \frac{\partial \theta}{\partial \zeta} \right), \quad (2.21)$$

where scaled versions of the material properties are given by

$$X = \hat{S} \frac{\theta_B - 1}{\theta_B - \theta}, \quad (2.22a)$$

$$k = 1 - X\Delta k, \quad (2.22b)$$

$$c = 1 - X\Delta c + \frac{\hat{L}}{\theta_B - \theta} X. \quad (2.22c)$$

Although (2.21) does not include any direct advective transport, the second term on the left-hand side is a pseudo-advection term proportional to  $q$  associated with the changing domain.

#### 2.4. Parameter values and approximations

Six dimensionless parameters characterise the problem. In this section, we give typical values or ranges for these parameters and discuss appropriate approximations. We also recast two parameters to better separate material properties (that are essentially fixed) from quantities that vary depending on environmental conditions. Throughout this section, we use material properties given in table 1 of Rees Jones & Worster (2014); see references therein for further discussion.

First, the difference between solid and liquid conductivities  $\Delta k = 1 - k_l/k_s \approx 0.76$ . This means that the thermal conductivity of ice is about four times higher than that of water, a significant difference. However, various MU-type models use a formula for the thermal conductivity of the form

$$\bar{k} = k_s + \beta S/T, \quad (2.23)$$

where  $\beta$  is an empirical constant. By comparing this expression with (2.2a) and (2.6), we see that the MU-type models are equivalent provided  $\Delta k = \beta/mk_s$ . Particular choices of parameters differ slightly between publications, so, as an example, we consider the default parameter values given in the CICE/Icepack documentation (Hunke *et al.* 2024a,b). These list  $\beta = 0.13 \text{ W m}^{-1} \text{ ppt}^{-1}$ ,  $m = 0.054 \text{ deg ppt}^{-1}$  and  $k_s = 2.03 \text{ W m}^{-1} \text{ deg}^{-1}$ , which combine to give  $\Delta k \approx 1.2$ . This is physically problematic in the framework of mushy-layer theory because  $\Delta k \leq 1$  by definition (2.3a). Indeed, the Icepack documentation casts doubt on the suitability of these parameter values based on experimental results (Hunke *et al.* 2024b). However, it appears not widely known that these default parameter values are inconsistent with mushy-layer theory. We comment more generally on this issue in the context of large-scale models in § 6.2.

Second, the difference between solid and liquid heat capacities  $\Delta c = 1 - c_l/c_s \approx -1.1$ . Equivalently, the heat capacity of water is about double that of ice. This is a significant difference. However, by inspecting (2.22c), we see that the magnitude of  $\Delta c$  should be compared with the role of latent heat since both appear multiplied by  $X$ . Indeed the ratio



of the second and third terms is

$$\frac{\Delta c}{\hat{L}/(\theta_B - \theta)} \leq \frac{\Delta c \theta_B}{\hat{L}} = \frac{c_s - c_l}{L}(-T_B), \quad (2.24)$$

where the inequality arises from the fact that  $\theta > 0$ . Even for quite strong cooling, e.g.  $T_B = -20^\circ\text{C}$ , the ratio in (2.24) is  $\lesssim 0.13$ . For numerical calculations, we will retain the parameter  $\Delta c$ . However, it only has a small effect on results and we will neglect it when carrying out analysis to reduce the number of parameters.

Third, the effective ice–ocean temperature difference  $\theta_e = c_l(T_l - T_0)/L \ll 1$ , because  $L/c_l \approx 77^\circ\text{C}$  and any temperature difference is typically less than a degree (and often much smaller). In some mushy-layer models of sea ice, this term still plays an important role, because it regularises the Stefan condition in the case that the liquid fraction  $X = 1$  at the interface (2.11). However, in our model with a fixed sea-ice salinity, it is reasonable to neglect  $\theta_e$  provided  $\hat{S}$  is not very close to 1 (which ensures the liquid fraction is not 1 at the interface). Formally, we need  $\theta_e \ll 1 - \hat{S}$ . For numerical calculations, we will use the representative value  $T_l - T_0 \approx 0.017^\circ\text{C}$ , which gives  $\theta_e \approx 2 \times 10^{-4}$ . For analytical calculations, we neglect this term as an excellent approximation.

Fourth, the effective latent heat or Stefan number  $\hat{L} = L/(c_s \Delta T) \gg 1$ , because  $L/c_s \approx 160^\circ\text{C}$  which is much greater than a typical temperature difference across the ice. For example, if  $\Delta T \approx 20^\circ\text{C}$ , then  $\hat{L} \approx 8$ . The definition of  $\hat{L}$  is convenient for simplifying and analysing the equations. However, one limitation of this formulation is that changing the cold atmospheric temperature  $T_B$ , which will vary depending on the environmental conditions, changes both  $\hat{L}$  and  $\theta_B$ . Therefore, we introduce an alternative effective latent heat

$$\hat{L}_0 = \frac{L}{c_s(-T_0)} \approx 83, \quad (2.25)$$

which, to an excellent approximation, is a fixed material property, because the freezing point of seawater is roughly constant (assuming its salinity does not vary much).

Fifth, the scaled cold atmospheric temperature  $\theta_B = -T_B/\Delta T > 1$ , which ensures that the atmospheric temperature is below the freezing point  $T_0$ . As  $T_B$  approaches  $T_0$ , the temperature differences  $\Delta T$  approaches zero, so  $\theta_B$  can be arbitrarily large. Thus, we introduce an alternative parameter

$$\theta_0 = (\theta_B - 1)^{-1} \equiv \frac{\Delta T}{-T_0}, \quad \Leftrightarrow \quad \theta_B = 1 + \theta_0^{-1}, \quad (2.26)$$

where the equivalence expresses  $\theta_0$  in terms of dimensional quantities. In a similar way to  $\hat{L}_0$ , it is convenient to scale against a fixed quantity. Thus  $\theta_0$  varies between 0 (when there is no freezing) and about 9.4 (when  $T_B = -20^\circ\text{C}$  and there is strong freezing). Unless otherwise stated, we take a default value  $\theta_0 \approx 9.4$ . Then the Stefan number can be rewritten

$$\hat{L} = \hat{L}_0 \theta_0^{-1}. \quad (2.27)$$

Thus, variation in  $\theta_0$  should be interpreted as representing variation in the environmental conditions, which in turn controls variation in  $\hat{L}$ . Combining the default values for  $\hat{L}_0$  and  $\theta_0$  gives a default value for  $\hat{L} \approx 8.3$ .

Sixth, the sea-ice salinity  $\hat{S}$  defined in (2.12) will lie between 0 and 1. In mushy-layer theory, the salinity is constant across the ice–ocean interface, so  $\hat{S} = 1$  at the interface. Equivalently, all the salt contained in seawater is initially incorporated into the sea ice as

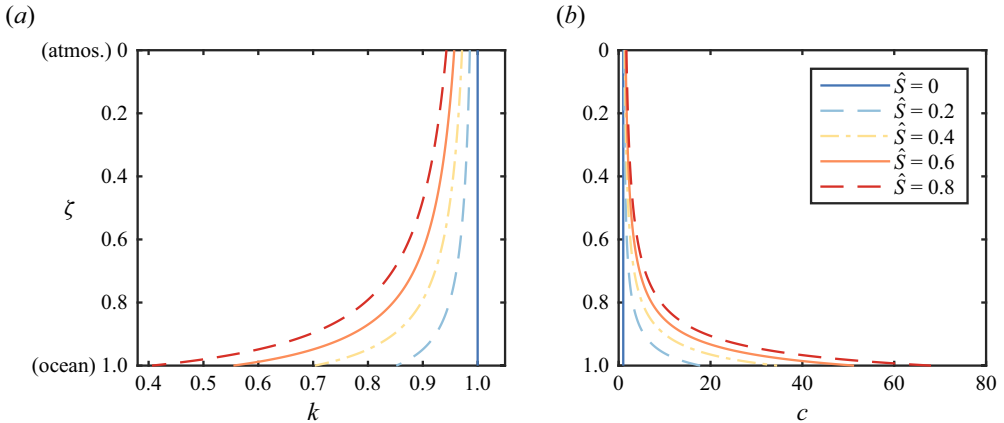


Figure 1. Depth dependence of the thermal properties of sea ice from atmosphere ( $\zeta = 0$ ) to ocean ( $\zeta = 1$ ). (a) The thermal conductivity and (b) the heat capacity of sea ice vary considerably with salinity  $\hat{S}$ . The depth dependence was calculated by assuming that temperature varied linearly with depth ( $\theta = \zeta$ ) in (2.22).

liquid brine inclusions (Notz & Worster 2008). Some laboratory experiments suggest that there is a delay of several hours before desalination begins (Wettlaufer, Worster & Huppert 1997). However, this is a relatively short time period and such a delay was not apparent in the field observations of Notz & Worster (2008). Within about 12 hours, sea ice appears to lose at least half the salt originally contained in seawater (Notz & Worster 2008; Thomas *et al.* 2020) so for all but the very initial stages of ice growth, it is reasonable to take  $\hat{S} \lesssim 0.5$ . For our results, we consider salinities between  $\hat{S} = 0$  (fresh ice) and  $\hat{S} = 0.8$  (very salty ice, in dimensional units about 28 ppt, which is much saltier than even very young ice is observed to be) to consider a very broad possible range.

The values of  $\Delta k$  and  $\Delta c$  ensure that the effective conductivity and heat capacity of sea ice vary considerably in sea ice (figure 1). Saltier ice is less thermally conductive because the liquid fraction is higher. However, saltier ice has a higher heat capacity. The fact that the heat capacity is much greater than 1 reflects the fact that the heat capacity (2.22c) is dominated by latent heat release.

## 2.5. Dimensional parameter values

The solution of the dimensionless problem only involves the dimensionless parameters introduced previously. However, to convert back to dimensional form, we additionally need the dimensional steady-state thickness estimate  $h_\infty$ .

In addition to the material properties given in table 1 of Rees Jones & Worster (2014), we need to specify a value of  $F_T$ ,  $T_0$  and  $T_B$ . We take  $F_T = 0.0013 \text{ J s}^{-1} \text{ cm}^{-2}$  and  $T_0 = -1.9^\circ \text{C}$ . This value of  $F_T$  is smaller than (about half) that used in Rees Jones & Worster (2014) and was chosen to achieve a sensible equilibrium thickness, comparable to Maykut & Untersteiner (1971). The value of  $F_T$  used is within the range observed by Wettlaufer (1991). For  $T_B$ , we consider two possible values.

- (i) For  $T_B = -20^\circ \text{C}$ , we obtain  $\Delta T = 18.1^\circ \text{C}$ , which gives rise to  $h_\infty = 280 \text{ cm}$  and, hence, a diffusive time scale  $h_\infty^2/\kappa_s = 7.7 \times 10^6 \text{ s}$  (or 89 days).
- (ii) For  $T_B = -10^\circ \text{C}$ , we obtain  $\Delta T = 8.1^\circ \text{C}$ , which gives rise to  $h_\infty = 130 \text{ cm}$  and, hence, a diffusive time scale  $h_\infty^2/\kappa_s = 1.5 \times 10^6 \text{ s}$  (or 18 days).

## 2.6. Equilibrium thickness

The ice grows and reaches an equilibrium (steady-state) thickness  $\hat{h}_\infty$  at which the growth rate factor  $q = 0$ . The temperature  $\theta = \theta(\zeta)$  alone. By (2.19), we observe that  $(k\theta')(1) = \hat{h}_\infty$ . The left-hand side of (2.21) is zero at steady state. Thus, by integrating the right-hand side once and applying the condition at  $\zeta = 1$ , we obtain

$$\left(1 - \hat{S}\Delta k \frac{\theta_B - 1}{\theta_B - \theta}\right) \frac{d\theta}{d\zeta} = \hat{h}_\infty, \quad (2.28)$$

where we used (2.22) to express  $k$ . This is a first-order separable equation with two boundary conditions ( $\theta(0) = 0$ ,  $\theta(1) = 1$ ) which allows us to determine the unknown parameter  $\hat{h}_\infty$ . We integrate again and apply the boundary conditions to obtain

$$\begin{aligned} \hat{h}_\infty &= 1 - \hat{S}\Delta k (\theta_B - 1) \log \frac{\theta_B}{\theta_B - 1}, \\ &= 1 - \hat{S}\Delta k \theta_0^{-1} \log(1 + \theta_0), \end{aligned} \quad (2.29)$$

where we used (2.26) to convert from  $\theta_B$  to  $\theta_0$ .

The equilibrium thickness calculated decreases linearly with salinity  $\hat{S}$ , which is driven by the thermal conductivity difference  $\Delta k$ . The dependence is also affected by the thermal parameter  $\theta_0$ . When  $\theta_0 \ll 1$ , we note that  $\theta_0^{-1} \log(1 + \theta_0) \sim 1 + O(\theta_0)$ . This gives  $\hat{h}_\infty \approx 1 - \hat{S}\Delta k$ , an estimate that could be derived using a simple zero-layer type of model of ice in which the temperature field  $\theta \approx \zeta$ . However, when  $\theta_0$  is larger, the sensitivity of equilibrium thickness to salinity is smaller. For example, when  $\theta_0 \approx 9.4$ , the largest value considered in § 2.4,  $\theta_0^{-1} \log(1 + \theta_0) \approx 0.25$ .

## 2.7. QS approximation

A crucial simplification we can make to the system of equations is to neglect the explicit time-dependence  $\partial\theta/\partial\tau$  in the heat equation (2.21). This is a major simplification because it reduces a PDE to an ODE. The resulting equations are still time-dependent because the ice thickness depends on time and this affects the solution via the definition of  $q$  in (2.19). For constant boundary conditions and when  $\hat{h} \ll 1$ , the QS solution is an exact solution of the full PDE. This is sometimes called a similarity solution, an idea used in previous analytical studies (Stefan 1891; Huppert & Worster 1985; Worster 1986). Thus, the QS approximation can be thought of as a generalisation of a similarity solution.

To motivate this approximation, consider the initial phase of ice growth (from an initial thickness of zero). We scaled the equations such that  $q = O(1)$  provided  $\hat{S} \neq 1$ , cf. (2.19). Then, by integrating (2.20),

$$\hat{h} \propto \sqrt{\frac{2\tau}{\hat{L}}}, \quad (2.30)$$

so the first term in the heat equation (2.21) is a factor of  $\tau$  smaller than the second term. Therefore, initially at least, we can guarantee that the explicit time dependence is negligible. Moreover, at later times, the system is likely to be evolving slowly anyway. We will test the practical effects of this approximation later by comparing a full solution of the PDE to the ODE (§ 5.3).

Under the QS approximation, the heat equation (2.21) reduces to a boundary-value problem (BVP)

$$-\frac{c\zeta q}{\hat{L}}\theta' = (k\theta')', \quad \theta(0) = 0, \quad \theta(1) = 1, \quad q = \frac{(k\theta')(1) - \hat{h}}{1 - \hat{S} + \theta_e}. \quad (2.31a-d)$$

Equation (2.31a) is a second-order ODE with an unknown parameter  $q$ , hence the three boundary conditions (2.31b–d). The left-hand side of (2.31a) is a pseudo-advection term associated with the change of coordinate system.

The BVP is coupled to an initial-value problem (IVP) for ice thickness (2.20). We define

$$\hat{y} = \hat{h}^2 \hat{L}/2, \quad (2.32)$$

so that the IVP has the simple form

$$\frac{d\hat{y}}{d\tau} = q, \quad \hat{y}(0) = 0. \quad (2.33)$$

The coupled BVP–IVP can be solved very straightforwardly using collocation methods for the BVP (Kierzenka & Shampine 2001) and Runge–Kutta methods for the IVP. We present an implementation based on the MATLAB `bvp4c` and `ode45` routine, respectively (see the data availability statement for a link to the code). Similar implementations are available in the SciPy library, for example.

### 3. Initial ice growth rate

In this section, we analyse the early stage of sea-ice growth from an initial thickness of zero. We focus on how the growth rate depends on the salinity of sea ice and its latent heat.

The initial ice thickness is zero ( $\hat{h} = 0$ ), so the BVP (2.31) simplifies to

$$-\frac{c\zeta q_0}{\hat{L}}\theta' = (k\theta')', \quad \theta(0) = 0, \quad \theta(1) = 1, \quad q_0 = \frac{(k\theta')(1)}{1 - \hat{S} + \theta_e}, \quad (3.1a-d)$$

where we introduce the notation  $q_0$  for the initial value of  $q$ . The solution of the BVP, and hence the value of  $q_0$ , will depend on all the material parameters of the system (§ 2.4). Our primary goal in this section is to analyse the role of salinity  $\hat{S}$  in controlling initial ice growth. We start by deriving analytical solutions valid when  $\hat{L} \gg 1$  (§ 3.1) and  $\hat{S} \ll 1$  (§ 3.2). This analytical approach elucidates the physical mechanisms at play. Then we will perform numerical calculations across the full parameter range (§ 3.3).

#### 3.1. Analytical solution when the Stefan number is large

The parameters of the system (§ 2.4) suggest various approximations that simplify the analysis. We take  $\Delta c = \theta_e = 0$  in this subsection and the next. In this subsection, we take  $\hat{S} = 0$  (fresh ice) and investigate the effect of latent heat in the limit that the Stefan number is large,  $\hat{L} \gg 1$ . Given that  $\hat{S} = 0$ , the parameters  $\Delta k$  and  $\theta_B$  do not affect the solution.

The Stefan problem when  $\hat{S} = 0$  is very well known so we only sketch the solution. The temperature

$$\theta = \frac{\operatorname{erf}(C\zeta)}{\operatorname{erf}(C)}, \quad (3.2)$$

where  $C = (q_0/2\hat{L})^{1/2}$  and  $q_0 = (2/\sqrt{\pi})C \exp(-C^2)/\operatorname{erf}(C)$ . By eliminating  $C$ , we obtain an implicit algebraic expression governing  $q_0(\hat{L})$ . Finally, by taking the limit

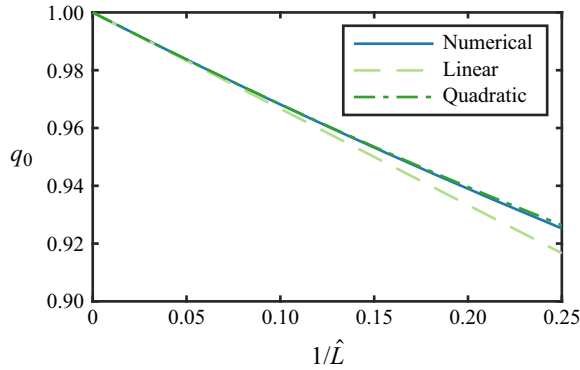


Figure 2. Dependence of initial growth rate factor  $q_0$  on the latent heat  $\hat{L}$  calculated numerically and asymptotically (3.3).

$\hat{L} \rightarrow \infty$  (in which  $C \rightarrow 0$ ), we obtain the asymptotic estimate

$$q_0 \sim 1 - \frac{1}{3} \frac{1}{\hat{L}} + \frac{7}{45} \frac{1}{\hat{L}^2} + O(\hat{L}^{-3}). \quad (3.3)$$

Figure 2 shows that the asymptotic estimate is extremely close to the full numerical solution throughout the parameter range of interest. Indeed, even the leading order estimate  $q_0 \sim 1$  has an error of less than about 4 % for  $\hat{L} > 8$  ( $1/\hat{L} < 0.125$ ), the geophysical range of interest identified in § 2.4.

The corresponding leading order solution  $\theta = \zeta$ , i.e. the temperature field is approximately linear through the ice. Thus models that assume a linear temperature profile such as the Semtner zero-layer model (Semtner 1976) are effective provided the latent heat is sufficiently large.

### 3.2. Analytical solution when the bulk salinity is small

We now extend the analysis to consider small but non-zero bulk salinity by investigating the limit  $\hat{S} \ll 1$ . We continue to make the assumption that  $\hat{L} \gg 1$  but the solution now depends additionally on the parameters  $\Delta k$  and  $\theta_B$ . As we discussed in § 1, one of the major developments in recent sea-ice modelling has been dynamically calculating the bulk salinity. But different models of bulk-salinity evolution seem to have little effect on ice thickness (Griewank & Notz 2013; Rees Jones & Worster 2014; Worster & Rees Jones 2015). Our goal is to understand the physical reasons for this limited sensitivity and explore how this is manifested in common large-scale sea-ice models.

The key idea is to decompose the temperature field

$$\theta \sim \zeta + \hat{S} \tilde{\theta}(\zeta) + O(\hat{S}^2, \hat{L}^{-1}), \quad (3.4)$$

where the perturbation temperature field  $\tilde{\theta}$  satisfies a second-order BVP subject to  $\tilde{\theta}(0) = \tilde{\theta}(1) = 0$ . This BVP is obtained by substituting (3.4) into (3.1) and equating terms of the same order in  $\hat{S}$  (i.e. we linearise the system in  $\hat{S}$ ).

We give full details in Appendix B. Here we explain the main physical simplifications involved. The liquid fraction  $X = \hat{S}(\theta_B - 1)/(\theta_B - \theta)$ , so to leading order  $X$  is proportional to  $\hat{S}$  and the temperature field in the denominator can be replaced by  $\theta \sim \zeta$ . Then the heat capacity ratio on the left-hand side of (3.1a) can be estimated by

$c/\hat{L} \sim X/(\theta_B - \zeta)$  for similar reasons. The thermal conductivity  $k = 1 - \Delta k X$  so there is a constant part (which must be retained), and a part that is proportional to  $X$ , and hence  $\hat{S}$ , so is retained too. Thus, it is important to consider how thermal conductivity varies with liquid fraction. Finally, the Stefan condition (3.1d) is linearised as follows

$$q_0 = \frac{(k\theta')(1)}{1 - \hat{S}} \sim 1 + \hat{S}[1 - \Delta k + \tilde{\theta}'(1)] + O(\hat{S}^2, \hat{L}^{-1}). \quad (3.5)$$

The term in square brackets includes three terms that control the sensitivity of the growth rate of ice to its salinity.

The first term comes from linearising the denominator of the expression for  $q_0$ . Physically, this term arises from the latent heat released at the ice–ocean interface. A larger  $\hat{S}$  increases the liquid fraction at the interface which reduces the latent heat liberated there which, in turn, increases the growth rate. That is, salty ice tends to grow quicker than fresher ice because there is less latent heat to be conducted away from the growing interface.

The second term comes from linearising the heat flux at the interface: considering the variation in thermal conductivity while retaining the leading order estimate  $\theta'(1) \sim 1$ . At the interface,  $\theta = 1$ , so the terms involving  $\theta_B$  cancel and we are left with a contribution  $-\Delta k$ . Physically, a higher  $\hat{S}$  increases the liquid fraction which reduces the thermal conductivity because liquid water is less conductive than ice. That is, salty ice would tend to grow slower than fresher ice because it is less thermally conductive.

The combination of the first and second terms is consistent with the prediction of a simple zero-layer type of model of ice. Worster & Rees Jones (2015) discussed the relative insensitivity of ice growth to salinity in terms of the competing effects of thermal conductivity and latent heat growth. Here, we give a clear quantification of that competition. In particular,

$$\frac{\partial q_0}{\partial \hat{S}} \approx 1 - \Delta k \approx 0.26. \quad (3.6)$$

Thus, the overall sensitivity of ice growth to salinity is rather weak because the latent heat and the thermal conductivity dependencies trade-off very strongly, even though individually they vary very strongly with salinity (see figure 1). Mathematically the weak sensitivity arises because the parameter group  $1 - \Delta k$  is small. Note that, from the definition of  $\Delta k$ , we have  $1 - \Delta k = k_l/k_s$ , so the weak sensitivity occurs in practice because  $k_l$  is much smaller than  $k_s$ .

Furthermore, we identify an additional term,  $\tilde{\theta}'(1)$ , which is the third term in the bracket of (3.5). This term also comes from linearising the heat flux at the interface, this time considering the changed temperature profile  $\tilde{\theta}(\zeta)$  through the ice while fixing the leading order estimate  $k = 1$ . Calculating this term is much more involved as it requires us to solve the BVP for  $\tilde{\theta}(\zeta)$ .

The total effect of all these terms can be found by calculating  $\tilde{\theta}'(1)$  and combining with the other terms (see Appendix B for details). We obtain the asymptotic estimate

$$q_0 \sim 1 + \hat{S}(\theta_B - 1) \left[ -2 - (2\theta_B - \Delta k) \log(1 - \theta_B^{-1}) \right] + O(\hat{S}^2, \hat{L}^{-1}). \quad (3.7)$$

This estimate differs from the zero-layer type estimate (3.6) in two main respects. It depends on  $\theta_B$  whereas the previous estimate is independent of this parameter. The dependence on  $\Delta k$  is also different. The connection between the estimates is clearer if we

### Thermodynamic growth of sea ice

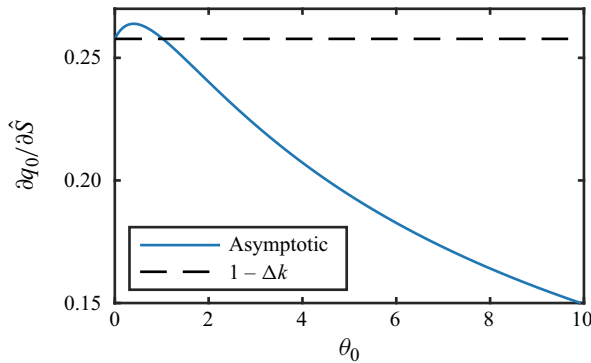


Figure 3. Sensitivity of the initial growth rate factor to salinity at small  $\hat{S}$  calculated asymptotically in the top line of (3.8). Note that the vertical axis does not begin at zero.

express equation (3.7) in terms of  $\theta_0$  using (2.26), and then rewrite as a sensitivity

$$\begin{aligned} \frac{\partial q_0}{\partial \hat{S}} &\sim \theta_0^{-1} \left[ -2 - (2 + 2\theta_0^{-1} - \Delta k) \log(1 + \theta_0) \right] + O(\hat{S}, \hat{L}^{-1}), \\ &\sim [1 - \Delta k] + O(\hat{S}, \hat{L}^{-1}, \theta_0), \end{aligned} \quad (3.8)$$

where the final result follows by taking the limit  $\theta_0 \rightarrow 0$ . Figure 3 shows that the sensitivity of sea-ice growth to salinity varies significantly with the cooling rate  $\theta_0$  across the parameter range of interest. The prediction of (3.8) is met at small  $\theta_0$ . However, for strong cooling conditions when  $\theta_0 = 10$ , the growth rate factor is about 40 % smaller than expected at small  $\theta_0$ , for example. Given that strong cooling (large  $\theta_0$ ) conditions are typical, this newly identified feedback mechanism associated with alteration to the thermal profile is significant.

### 3.3. Numerical results

The asymptotic results were derived by assuming that the salinity of ice was very small  $\hat{S} \ll 1$ . However, in practice, we are interested in a range of salinities  $0 \leq \hat{S} \leq 0.8$  as discussed in § 2.4. Therefore, we solve for the initial growth rate factor  $q_0$  numerically and compare with the asymptotic predictions

Figure 4 shows the dependence of the initial growth rate factor  $q_0$  on salinity  $\hat{S}$  according to various different models. The darker blue curves are the main results from our QS model, with  $\Delta k = 0.74$ , which is the best estimate for this parameter (§ 2.4). The corresponding asymptotic predictions agree with the numerical results in the limit of small  $\hat{S}$  and are a reasonable approximation for  $\hat{S} \lesssim 0.4$ . In practice, this corresponds to a dimensional salinity of about 14 ppt, so would be relevant to all but the earliest stages of ice growth. Nevertheless, the numerical results do diverge more sharply at higher salinity, with the growth rate factor exceeding that predicted asymptotically.

We also plot predictions from zero-layer type models in a lighter green colour, both the full calculation (solid) and the asymptotic limit from (3.6) (dashed). These both over-predict the ice growth rate, for the reasons discussed in the previous section. Moreover, the asymptotic limit diverges markedly from the full zero-layer calculation and is a poor approximation for  $\hat{S} \gtrsim 0.1$ . So even though the asymptotic zero-layer model appears to be a good model, this is coincidental.



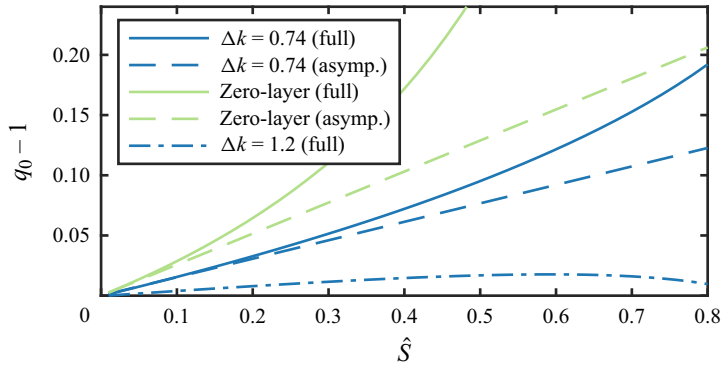


Figure 4. Dependence of initial growth rate factor  $q_0$  on the latent heat  $\hat{S}$ . The solid blue curve corresponds to the full numerical solution with our best estimate of the value of  $\Delta k$ . This approaches the asymptotic prediction (abbreviated ‘asympt.’ in the legend) as  $\hat{S} \rightarrow 0$  (blue dashed curve). The dot-dashed curve shows results for a larger value of  $\Delta k$ . Lighter, green curves denote the predictions of zero-layer models (solid curve shows the full model while the dashed curve is its asymptotic limit as  $\hat{S} \rightarrow 0$ ). This figure was computed with  $\hat{L} = 10^3$ ,  $\Delta c = \theta_e = 0$  to enable direct comparison with the asymptotic theory. These simplifications are tested in figure 5.

The above calculations, including the zero-layer results, were all made with  $\Delta k = 0.74$ . However, in § 2.4, we showed that  $\Delta k \approx 1.2$  in MU-type models such as CICE/Icepack (Hunke *et al.* 2024a,b). Thus, we also plot the numerical solution for the higher value of  $\Delta k = 1.2$ . It has a much weaker dependence on  $\hat{S}$  because the reduction in growth rate caused by thermal conductivity variation is made stronger.

In summary, all the models we presented agree with the general idea that the sensitivity to salinity is rather weak. The zero-layer model over-predicts the sensitivity while the high- $\Delta k$  model implemented as the default parameter choice in CICE/Icepack tends to under-predict the sensitivity.

In figure 5, we show more completely the dependence of the growth rate factor on the environmentally varying parameters of the system ( $\theta_0, \hat{S}$ ). Comparing panels (a,c), we see that the basic trends found numerically are consistent with the asymptotic analysis across the whole parameter space explored. Comparing panels (a,b) shows that relaxing the assumptions that  $\Delta c = 0$  and  $\theta_e = 0$  makes almost no difference to results, so this was a good assumption across the full parameter regime considered. Thus, the asymptotic analysis (panel c) and the physical mechanisms identified using it (§ 3.2) explain why the initial growth rate varies very weakly with salinity.

To conclude, the weak effect on relative growth rate is not only caused by the relatively low salinity  $\hat{S}$  (and, hence, low liquid fraction). For example, even a relatively high salinity ( $\hat{S} = 0.5$ , 50 % of the ocean seawater salinity) corresponds to  $q_0 - 1 \approx 0.1$ , which is about a 10 % difference in growth rate factor. Thus, the physical mechanisms, first the trade-off in thermal properties (conductivity/latent heat capacity) and second the feedback on temperature profile (analysed asymptotically in § 3.2), are crucial to understanding the role of salinity. In the next section, we investigate how this feeds through to the evolution of ice thickness.

#### 4. Later-stage ice growth rate and thickness evolution

As the ice continues to grow, the heat flux from the ocean gradually plays a greater role slowing the ice growth until the thickness reaches a steady state (assuming constant

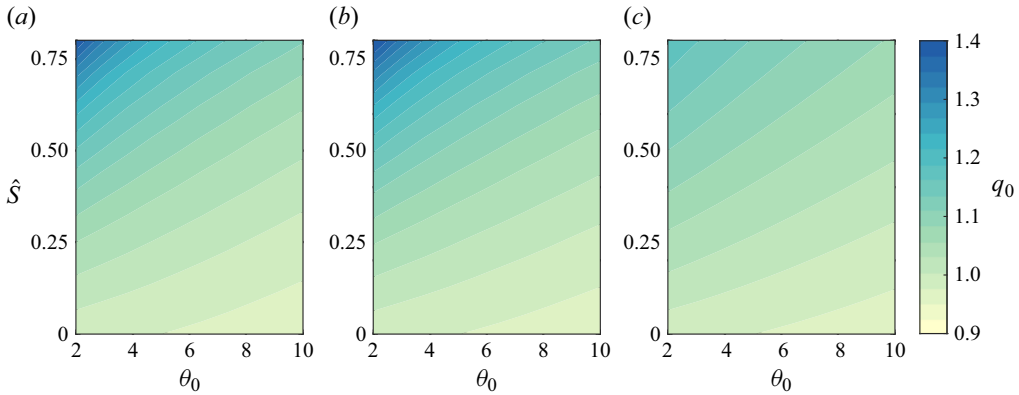


Figure 5. Dependence of the initial growth rate factor on external parameters. (a) Full numerical results with standard material parameter values. (b) Simplified numerical results ( $\Delta c = 0$  and  $\theta_e = 0$ ). (c) Asymptotic results based on the combination of (3.3) for the dependence on  $\hat{L}$  (where  $\hat{L} = \hat{L}_0 \theta_0^{-1}$  from (2.27)), and (3.7) for the dependence on  $\hat{S}$ . Note that we only plot  $\theta_0 \geq 2$  to focus on the parameter regime of geophysical interest. For smaller values  $\theta_0 \geq 2$ ,  $q_0$  increases rapidly in both sets of numerical calculations.

forcing, something we revisit in § 5). In this section, we calculate how the growth rate factor  $q$  depends on the ice thickness and then use this to determine the evolution of the ice thickness. We show that the sensitivity of the growth rate to salinity reverses sign, so saltier ice grows slower.

#### 4.1. Effect of ice thickness on the growth rate factor

Under the QS approximation (§ 2.7), the problem of calculating the ice growth rate factor does not depend on the evolution of the ice thickness, only the thickness at a given time. Thus, we now solve the full BVP (2.31) and denote the growth rate factor  $q(\hat{h})$ . This notation suppresses the dependence on all the material parameters of the system. Note that  $q_0 = q(\hat{h} = 0)$ . However, we can not simply take our solutions for  $q_0$  and find  $q$  by using the Stefan condition (2.31d), because  $q$  also appears in the heat equation (2.31a).

Numerically, we observe that the  $q(\hat{h})$  varies approximately linearly with  $\hat{h}$ . Figure 6 shows that this approximation holds very well across the full range of  $\hat{h} \in [0, 1]$  for parameter values that span the range of interest. While a linear dependence on  $\hat{h}$  might be anticipated from (2.31d), the slope is not consistent with  $(1 - \hat{S} + \theta_e)^{-1}$ . This is because the temperature profile itself also changes with  $\hat{h}$ .

Motivated by the observed linear trend in figure 6, we introduce the linear approximation

$$q(\hat{h}) \approx q_0 - q_1 \hat{h}, \quad (4.1)$$

where  $q_0$  and  $q_1$  depend on the system parameters but not  $\hat{h}$ . We calculate  $q_1$  by computing  $q$  at a very small value of  $\hat{h}$  to input, along with  $q_0$ , into a finite difference approximation of the (negative) slope at  $\hat{h} = 0$ .

Figure 7 shows that  $q_1$  (panel b) has a similar parametric dependence as  $q_0$  (panel a). In particular,  $q_1$  increases strongly with salinity. Indeed the dependence of  $q_1$  on salinity is stronger than that of  $q_0$ . The practical implication is that  $q(\hat{h})$  can decrease with salinity rather than increase. Figure 7(c) shows that at small  $\hat{h} \lesssim 0.4$ , the growth rate factor increases with  $\hat{S}$  (consistent with the initial growth rate sensitivity found in § 3.2)

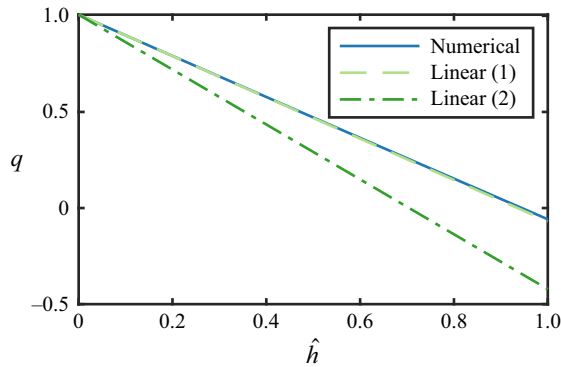


Figure 6. Dependence of growth rate factor  $q$  on the thickness  $\hat{h}$  for  $\hat{S} = 0.3$ . The solid blue curve corresponds to the full numerical solution. The dashed light green line shows a first linear approximation given by (4.1). This agrees very well with the full numerical solution. The dot-dashed darker green line shows a second alternative linear approximation  $q = q_0 - \hat{h}/(1 - \hat{S} + \theta_e)$  which does not agree with the numerical calculation.

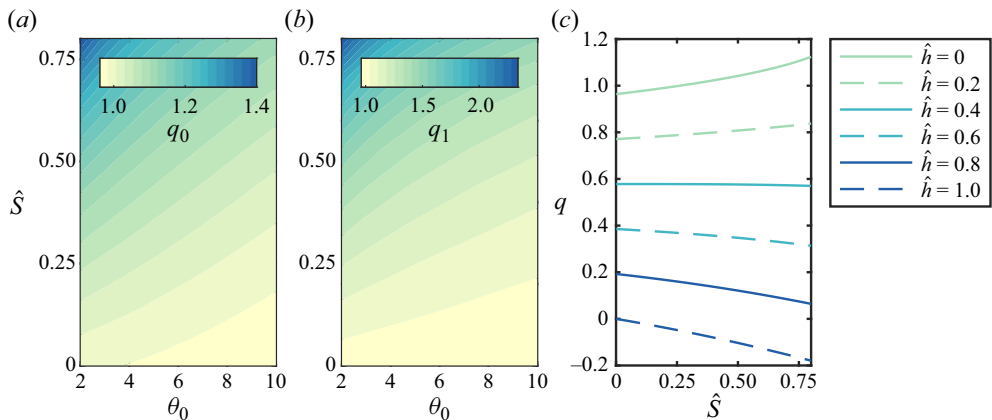


Figure 7. Dependence of the growth rate factor on external parameters. Panels (a,b) show how the constant and linear terms in (4.1), respectively, depend on external parameters. These parameters are the same as the ‘full numerics’ parameters of figure 5. Panel (c) shows the resulting sensitivity of the growth rate factor to salinity at increasing ice thickness. A negative  $q$  corresponds to thickness decaying towards its equilibrium state.

but for larger  $\hat{h} \gtrsim 0.4$ , the trend reverses. This reversed trend is consistent with the fact that the equilibrium (steady-state) thickness decreases with salinity (see (2.29) in § 2.6).

Physically the reversal in sensitivity to salinity can be understood by considering the changing relative importance of the different processes that control the sensitivity to salinity. As the ice grows, the growth rate reduces, which reduces the importance of the latent heat sensitivity to salinity (recall that saltier ice grows faster as less latent heat is released by saltier ice). The turbulent ocean heat flux (a constant, independent of salinity) becomes relatively more important. The conductive heat flux reduces, but at a slower rate than the latent heat production reduces. Indeed, as the thickness approaches a steady state (§ 2.6), the latent heat production is negligible and there is a balance between turbulent ocean heat flux and conductive heat flux through the ice. Thus, the fact that the saltier ice is less thermally conductive eventually dominates the overall sensitivity to salinity, such that saltier ice grows slower beyond  $\hat{h} \gtrsim 0.4$ .

#### 4.2. Ice thickness evolution

As the ice grows  $\hat{h}$  increases, so while *initially* saltier ice grows faster, *subsequently* saltier ice grows slower. This is a further reason that the sensitivity of ice growth to ice salinity is small. We next investigate the net result by calculating the thickness evolution using (2.33). If the growth rate factor has the simple linear form given by (4.1), then the evolution equation becomes

$$\frac{d\hat{y}}{d\tau} = q_0 - (2q_1^2/\hat{L})^{1/2}\hat{y}^{1/2}, \quad \hat{y}(0) = 0, \quad (4.2)$$

where we used (2.32) to convert between scaled thickness  $\hat{h}$  and scaled squared thickness  $\hat{y}$ . This is a separable equation and the analytical solution can be written in terms of the product–logarithm function (sometimes called the Lambert  $W$ -function). This function is defined as the root  $w = W$  of  $we^w = z$  (the principle value, which satisfies  $W \geq -1$ , is the relevant root here).

We express the analytical solution in terms of the thickness

$$\hat{h} = \frac{q_0}{q_1} \left\{ 1 + W \left[ -\exp \left( \frac{-\tau q_1^2}{\hat{L} q_0} - 1 \right) \right] \right\}. \quad (4.3)$$

To the best of the author's knowledge, this expression is a new analytical estimate of the growth trajectory of sea ice. A related expression is given in an implicit form in Worster (2000) and in the PhD thesis Notz (2005) but these earlier expressions are based on a zero-layer model for ice growth.

Figure 8 shows that the thickness is initially proportional to  $\tau^{1/2}$  (see the inset), as is typical for Stefan problems (Worster 2000). This comes from taking  $q_0 \approx 1$  from (3.7), which is valid at small  $\hat{S}$  and large  $\hat{L}$ . However, the thickness diverges markedly from this initial growth even by  $\tau = 1$ . The growth slows and approaches a steady state as  $\tau \rightarrow \infty$ . The new analytical solution from (4.3) is an excellent approximation to the full numerical solution across the full range of times considered. We plot results for two values of the ice salinity as examples. The initial growth of the saltier ice is slightly faster (but the curves are virtually indistinguishable). At late times, the saltier ice reaches a smaller thickness, consistent with the growth rate factor being a decreasing function of salinity once  $\hat{h} \gtrsim 0.4$ , as shown in figure 7(c). Thus, the competing sensitivity of growth to salinity at small vs large thickness is an additional reason why the overall ice thickness is relatively insensitive to salinity. For practical purposes, the calculations with different salinities are virtually indistinguishable up to about  $\tau \approx 5$ , which dimensionally corresponds to a period of at least about 100 days (based on the  $T_B = -10^\circ\text{C}$  conversion in § 2.5). This is a remarkable degree of insensitivity in the context of the significant variation in the thermal properties of ice between these salinities.

#### 5. Effect of time-dependent forcing and the validity of the QS approximation

Sea ice grows in highly variable environmental conditions. In this section, we progressively relax our assumptions of conditions being fixed. First, we consider the effect of variable atmospheric conditions (§ 5.1). Second, we consider the effect of variable salinity (§ 5.2). Third, and most significantly, we relax the QS approximation and compare solutions based on solving the full PDE system to solutions based on our QS approximation (§ 5.3).

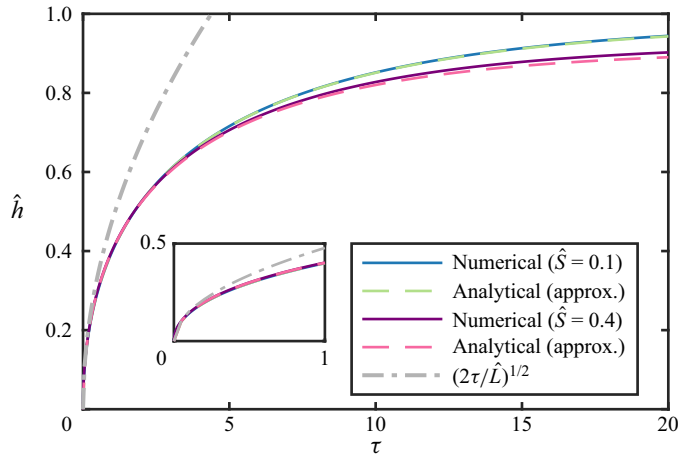


Figure 8. Ice thickness evolution calculated according to the numerical model at two different salinities. Dashed curves show the corresponding analytical approximation from (4.3), which are extremely close to the numerical curves. The dot-dashed curve shows an approximation to the initial growth based on  $q_0 \approx 1$  from (3.3). The inset shows the same data over the initial phase of growth.

### 5.1. Time-dependent atmospheric temperature

Variable atmospheric conditions are an important factor in sea-ice growth. We adjust the boundary condition at the ice–atmosphere interface. We retain the same non-dimensionalisation but interpret  $T_B$  as the long-term average boundary temperature. In dimensionless variables, the only change to the model is that

$$\theta(0) = \hat{g}(\tau), \quad (5.1)$$

where  $\hat{g}(\tau)$  represents the time-dependent boundary temperature. Within the QS framework, the growth rate factor only depends on the value of  $\hat{g}$  at a particular time, so we denote this dependence  $q(\hat{h}, \hat{g})$ , again suppressing the dependence on material properties.

Figure 9(a) shows that  $q$  decreases approximately linearly with  $\hat{g}$ . A higher value of  $\hat{g}$  corresponds to a higher (warmer) atmospheric temperature so slower ice growth. We introduce the approximation

$$q(\hat{h}, \hat{g}) \approx q_0 - q_1 \hat{h} - q_2 \hat{g}, \quad (5.2)$$

where  $q_2$  is estimated in an analogous way to  $q_1$ . A naïve, and rather good estimate of  $q_2$  can be obtained by substituting the zero-layer estimate  $\theta'(1) = 1 - \hat{g}$  into (2.31d), which gives

$$q(0, \hat{g}) \approx q_0(1 - \hat{g}), \quad (5.3)$$

or  $q_2 \approx q_0$ . Figure 9(b) shows that  $q_2$  varies only weakly with the external parameters and does so in a similar pattern to  $q_0$ , although the approximation  $q_2 \approx q_0$  is not valid uniformly (compare figure 5a).

We next consider the effect on the trajectory of ice thickness by solving the IVP (2.33) that governs its evolution. The full equation requires numerical solution. However, if we

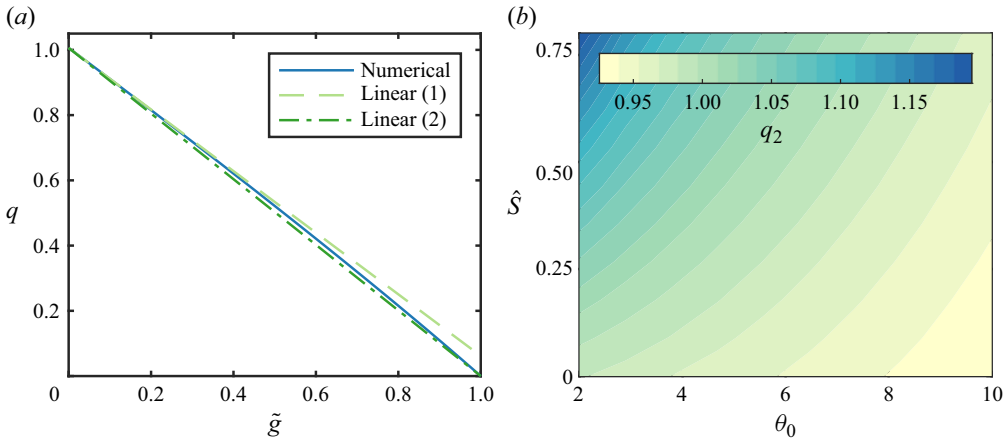


Figure 9. (a) Approximately linear dependence of the growth rate factor on  $\hat{g}$  for  $\hat{h} = 0$  and  $\hat{S} = 0.3$ . The first linear model (1) is based on numerical estimation of  $q_2$  at small  $\hat{g}$  as given by (5.2). The second linear model (2), based on a zero-layer model, is given by (5.3). (b) The full parameter dependence of the slope  $q_2$ .

adopt the linearisation (5.2) and take  $\hat{g} = \Delta g \hat{g}(\tau)$  where  $\Delta g \ll 1$ , then we find

$$\frac{d\hat{y}}{d\tau} = q_0 - q_1(2/\hat{L})^{1/2}\hat{y}^{1/2} - q_2\Delta g\hat{g}(\tau), \quad \hat{y}(0) = 0. \quad (5.4)$$

This equation can be linearised about the solution for  $\Delta g = 0$  (i.e. the solution we obtained in § 4.2). We let  $\hat{y} = \hat{y}_0 + \Delta g\hat{y}_1$ , then

$$\frac{d\hat{y}_1}{d\tau} = -q_2\hat{g}(\tau) + q_1\left(\frac{1}{2\hat{L}}\right)^{1/2}\frac{\hat{y}_1}{\hat{y}_0^{1/2}} + O(\Delta g), \quad \hat{y}_1(0) = 0. \quad (5.5)$$

Note that the quotient is well-behaved in the limit that  $\tau \rightarrow 0$ . Both the numerator and denominator tend to zero, but by l'Hôpital's rule,

$$\lim_{\tau \rightarrow 0} \frac{\hat{y}_1}{\hat{y}_0^{1/2}} = \lim_{\tau \rightarrow 0} \frac{\hat{y}_1'}{\frac{1}{2}\hat{y}_0'\hat{y}_0^{-1/2}} = \lim_{\tau \rightarrow 0} \frac{-q_2\hat{g}(0)}{\frac{1}{2}q_0}\hat{y}_0^{1/2} = 0, \quad (5.6)$$

where, in the second expression, a prime denotes a derivative with respect to  $\tau$ . For high latent heat  $\hat{L} \gg 1$ , the evolution equation for  $\hat{y}$  has a simple form:

$$\frac{d\hat{y}_1}{d\tau} = -q_2\hat{g}(\tau) + O(\Delta g, \hat{L}^{-1/2}), \quad \hat{y}_1(0) = 0. \quad (5.7)$$

We use these ideas to propose three solutions to the ice-thickness evolution equation:

- (i) a numerical solution to the IVP with the full  $q(\hat{h}, \hat{g})$ ;
- (ii) a numerical solution to the IVP with the linearised form (5.2);
- (iii) an analytical solution to the IVP based on (5.7).

Figure 10 shows the ice-thickness evolution for a sinusoidal forcing  $\hat{g} = \Delta g \sin(\omega\tau)$ , where  $\omega$  is the angular frequency. While realistic forcing would contain a large spectrum of frequencies, using a simple sinusoidal forcing allows us to test the success of the various approximations we introduced as a function of frequency. For intermediate and

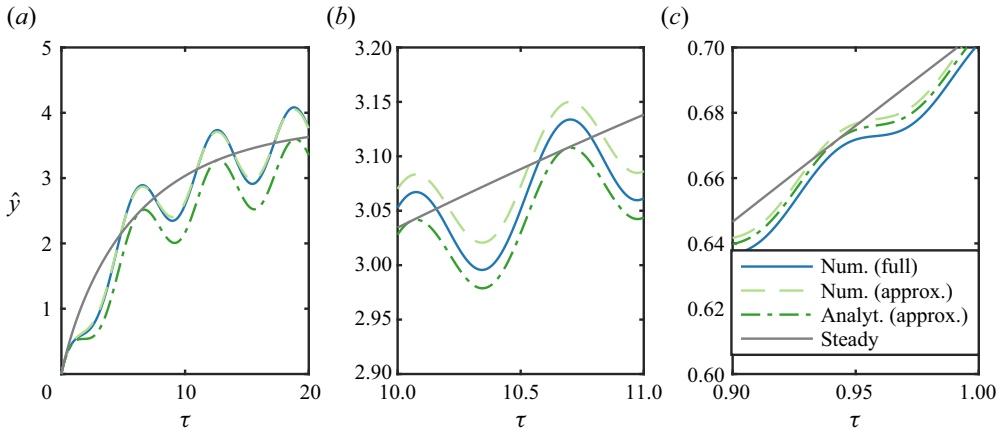


Figure 10. The evolution of ice plotted in terms of the squared thickness scale  $\hat{y} = \hat{h}^2 \hat{L}/2$  under sinusoidal atmospheric temperature variation  $\hat{g} = \Delta g \sin(\omega\tau)$  for  $\hat{S} = 0.3$ . In all panels  $\Delta g = 0.5$  to allow us to test the success of the approximate solutions beyond the  $\Delta g \ll 1$  limit in which they are derived. The panels show different forcing frequencies: (a) low frequency,  $\omega = 1$ ; (b) intermediate frequency,  $\omega = 10$ ; and (c) high frequency,  $\omega = 100$ . For the latter plots, we restrict the  $\tau$  axis range to show a representative part of the solution. Solid blue curve shows the full numerical solution, referred to as (i) in the main text. Dashed green curves show an approximate numerical solution (ii). Dot-dashed dark green curves show an analytical approximation (iii). Solid grey curves show the steady solution equivalent to (4.3).

high frequency ( $\omega = \{10, 100\}$ , corresponding, roughly, to sub-fortnightly time periods) all the approximations we introduced agree very well with the full numerical solution. (To be more precise, for the  $T_B = -10^\circ\text{C}$  conversion in § 2.5,  $\omega = 10$  corresponds to a period of 13 days.) For such frequencies, the basic behaviour can be most easily seen by integrating (5.7) which gives

$$\hat{y}_1 \approx \frac{q_2 \Delta g}{\omega} [\cos(\omega\tau) - 1]. \quad (5.8)$$

The growth rate is anti-phase with the forcing (because a peak in boundary temperature corresponds to a trough in growth rate). Then  $\hat{y}$  lags behind the peak in growth rate by a quarter of a cycle. For longer-term variability (e.g.  $\omega = 1$ ), the approximations (i)/(ii) agree well. However, there is a more significant departure from (iii). This is expected because  $\hat{y} \propto \omega^{-1}$ , so the  $O(\hat{L}^{-1/2})$  term neglected in deriving (5.7) will be smaller at high frequency than at low frequency. Similar behaviour has been observed in experimental systems with analogous behaviour (Ding, Wells & Zhong 2019).

### 5.2. Time-dependent salinity

We next investigate the effect of time-dependent salinity on ice growth. The evolution of the salinity profile is complex. Here, we investigate a simple prescribed time-dependent salinity to assess whether or not it has a large effect on ice growth. In particular, we let

$$\hat{S}(\tau) = \hat{S}_2 + (\hat{S}_1 - \hat{S}_2) \exp(-\tau/\tau_d), \quad (5.9)$$

where  $\hat{S}_1$  is the initial salinity,  $\hat{S}_2$  is the late-time salinity and  $\tau_d$  is the desalination time scale over which the salinity evolves. This type of exponential relaxation has been used previously by Vancoppenolle *et al.* (2009) and then used as the ‘slow mode’ of gravity



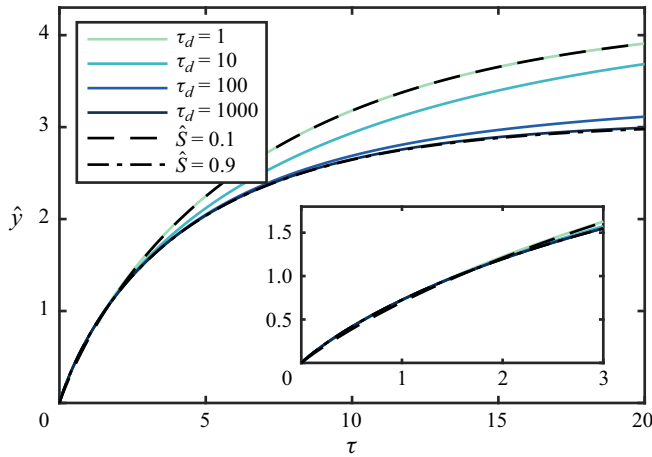


Figure 11. Ice growth plotted in terms of the squared thickness scale  $\hat{y} = \hat{h}^2 \hat{L}/2$  with time-dependent prescribed salinity according to (5.9) with initial salinity  $\hat{S}_1 = 0.9$  and late-time salinity  $\hat{S}_2 = 0.1$ . The solid curves correspond to different desalination timescales. The dot-dashed and dashed curves are constant-salinity calculations corresponding to the initial and late-time salinity, respectively. The inset shows the early time behaviour in which all the curves are almost indistinguishable. Close inspection shows that the  $\hat{S} = 0.1$  dashed curve is lowest early on, while the  $\hat{S} = 0.9$  dot-dashed curve is lowest at late times.

drainage by Turner *et al.* (2013). While it does not arise from any particular physical model of desalination, it is a simple functional form to explore.

Figure 11 compares the thickness evolution with a constant salinity (corresponding to either the initial or late-time salinity) with that with an evolving salinity. We look at an extreme example with a high initial salinity  $\hat{S}_1 = 0.9$  and low late-time salinity  $\hat{S}_2 = 0.1$  in order to consider a significant salinity drop. With a relatively rapid desalination time scale  $\tau_d \leq 1$ , the thickness is extremely close to a fixed salinity model with the prescribed late-time salinity. For longer desalination timescales, the salinity remains higher for longer. The thickness increases more slowly. For extremely long desalination timescales  $\tau_d = 100, 1000$ , much longer than the maximum  $\tau$  considered, the thickness evolution is close to a fixed salinity with the prescribed initial salinity.

In practice, we expect ice to desalinate significantly within the 18 days of growth that corresponds in dimensionless units to  $\tau = 1$  (for the  $T_B = -10^\circ\text{C}$  conversion in § 2.5, and even lower  $\tau$  for colder  $T_B$ ), so fixed-salinity models with the late-time salinity are likely to be excellent approximations. A 20-day desalination time scale was previously used for the winter by Vancoppenolle *et al.* (2009). Moreover, all the models give extremely similar results (see the inset plot looking up to  $\tau = 3$  which corresponds approximately to the first 2 months of growth). Later stages of growth are sensitive to the later-time salinity value.

Although the QS model we developed cannot consider the full dynamic evolution of salinity, it could, in principle, be extended to consider salinity profiles of the separable form

$$\hat{S} = r(\tau)s(\zeta), \quad (5.10)$$

where  $r$  and  $s$  are given functions. However, caution is needed as the assumptions used to justify the heat equation (2.8) would not be formally valid, as described in Appendix A.

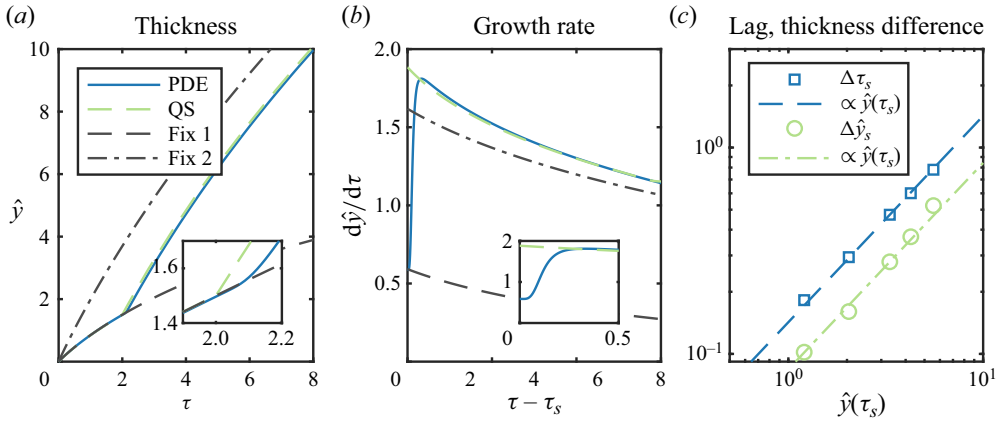


Figure 12. Ice growth calculated by the full PDE compared against the QS approximation. Panel (a) shows the evolution of  $\hat{y} = \hat{h}^2 \hat{L}/2$  for the PDE and QS models, as well as for two fixed temperature calculations (1, fixed at the initial atmospheric temperature; 2, fixed at the temperature after the switch occurs). The switch occurs at  $\tau_s = 2$ . Panel (b) shows the growth rate for the same example as panel (a). Insets of both panels highlight the behaviour around the switching time. Such experiments are repeated at a series of switching times. Panel (c) shows the results of a series of experiments with  $\tau_s = 1, 2, 4, 6$  and  $10$ . It shows the lag  $\Delta\tau_s$  before the growth rate of the PDE catches up with that of the QS model. It also shows the maximum absolute difference in  $\hat{y}$  after the switching time between the PDE and QS models denoted  $\Delta\hat{y}_s$ . Linear fits to the data are shown.

### 5.3. Non-QS effects

Finally, and most importantly, we consider the limitations of the major simplification introduced in this study, the QS approximation (§ 2.7). For fixed boundary conditions and an initial temperature profile consistent with that calculated within the QS approximation, the full PDE solution is identical to the QS solution. To provide a strong test of the QS solution, we perform experiments with a step change in the atmospheric boundary temperature at a given time  $\tau_s$ . In dimensional units, we switch from  $T_B = -10^\circ\text{C}$  to  $T_B = -20^\circ\text{C}$ . A step change is a more challenging test than the sinusoidal forcing considered in § 5.1. The salinity value used in these experiments was  $\hat{S} \approx 0.56$ , corresponding to 20 ppt. The non-dimensionalisation of the temperature is based on the initial  $T_B$  which gives  $\theta_0 \approx 4.2$  and  $\hat{L} \approx 20$ .

Figure 12(a,b) shows an example with a switching time  $\tau_s = 2$ . This corresponds to a dimensional time of 36 days, since we non-dimensionalise with respect to the initial value  $T_B = -10^\circ\text{C}$ , which corresponds to a diffusive time scale of 18 days (§ 2.5). The PDE and QS models agree extremely closely. For reference, fixed atmospheric temperature models with the before and after switch temperatures are also plotted. After the switch, the atmospheric temperature is much colder so the ice thickness increases more rapidly. In the QS model, the growth rate increases instantaneously. In the full PDE calculations, the growth rate increases rapidly (but not instantaneously) before catching up with the QS model over a switching lag time  $\Delta\tau_s$ . After this time, the growth rate of the PDE model is slightly faster than the QS because the thickness is slightly smaller. The absolute differences between the PDE and QS models in terms of thickness are very small.

The switching lag depends on the thickness around the time the switch occurs. Figure 12(c) shows the results of a series of experiments at different switching times. We observe that the lag is proportional to the value of the square of the ice thickness at the switching time, i.e.  $\Delta\tau_s \propto \hat{y}(\tau_s)$ . This is because the lag corresponds to the time it

takes for the cooling at the ice–atmosphere interface to diffuse across the full depth of the ice to the ice–ocean interface. A similar diffusive lag was observed experimentally by Ding *et al.* (2019). In our dimensionless units,  $\Delta\tau_s \propto [\hat{h}(\tau_s)]^2 \propto \hat{y}(\tau_s)$ . During this period of slower growth for the PDE model, slightly less ice grows. We denote the maximum absolute difference in  $\hat{y}$  between the PDE and QS models as  $\Delta y_s$ . We observe that  $\Delta\hat{y}_s \propto \Delta\tau_s \propto \hat{y}(\tau_s)$ . The first proportionality assumes that  $d\hat{y}/d\tau$  is approximately independent of switching time. While this is only an approximation, across the range considered in figure 12(c), the discrepancy is within about  $\pm 15\%$ , so the dot-dashed linear fit matches the calculated  $\Delta y_s$  well. Thus, although the lag increases with switching time, and the square thickness change  $\Delta\hat{y}_s$  increases too, the proportionate change  $\Delta\hat{y}_s/\hat{y}(\tau_s)$  does not increase. Therefore, the QS model remains an effective approximation to the PDE model for any switching time.

This was a strong test of the QS model. In practice, changes in atmospheric temperature will occur in both directions (not just a sudden cooling), which would partly offset each other. Furthermore, more realistic changes would occur more gradually than the instantaneous switch tested here. Thus, it is reasonable to expect the QS model to perform even better under more realistic forcing scenarios.

## 6. Discussion and implications

This study was designed to examine and explain the observed weak sensitivity of thermodynamic sea-ice growth to salinity observed in studies with a range of fixed-salinity profiles (e.g. Vancoppenolle *et al.* 2005) and in studies with dynamic-salinity profiles (e.g. Griewank & Notz 2013; Rees Jones & Worster 2014). This weak sensitivity occurs despite the strong sensitivity of the thermal properties (figure 1). There is an obvious basic reason, the sea-ice salinity is low so the solid fraction is high and the thermal properties are close to that of pure ice. However, the insensitivity persists even when the salinity is not very low (relative to the salinity of seawater). To explain the insensitivity, we identified the three main mechanisms described below.

### 6.1. Three mechanisms that explain why ice growth rate is insensitive to salinity

- 1. Trade-off between thermal conductivity and latent heat capacity.** Saltier ice has a higher liquid fraction and, hence, a lower thermal conductivity, which leads it to grow slower. However, a higher liquid fraction also means less latent heat needs to be conducted away as the ice grows, which leads it to grow faster. This competition was described in Worster & Rees Jones (2015). In this study, we give a detailed quantification and derive excellent analytical estimates for the effect (cf. figure 4).
- 2. Feedback on the thermal profile within the ice.** Our previous estimates of the sensitivity to salinity assumed a linear thermal profile (Worster & Rees Jones 2015), as per zero-layer Semtner models (Semtner 1976). In this study, we show that feedback on the thermal profile, which produces a nonlinear profile, reduces the sensitivity to salinity further and introduces a sensitivity to the cooling factor (the ratio of the temperature difference across the ice to the freezing point of seawater), as shown by figures 3 and 5.
- 3. Opposite sensitivity of thicker ice vs thinner ice.** Saltier ice grows faster when the ice is thin, but saltier ice grows slower when the ice is thicker. This reversed sensitivity can be understood by considering the relative importance of the three mechanisms that determine the growth rate and their separate sensitivities to salinity. As well as the mechanisms described in reason 1, the turbulent ocean heat flux is a constant,

independent of salinity. As the ice grows thicker, the latent heat mechanism becomes relatively less important (indeed at the steady state, equilibrium thickness, it can be neglected entirely). Thus, when the ice is sufficiently thick, the sensitivity to salinity reverses, and saltier ice grows slower (figures 6 and 7). As the thickness evolves from zero towards the equilibrium thickness, the sensitivities oppose each other, leading to an even smaller net sensitivity (figure 8).

## 6.2. Implications for large-scale sea-ice modelling

Recently, there has been a move towards using ‘dynamic salinity’ sea-ice models, as described in the introduction (§ 1). In terms of the ice-thickness evolution alone, these models behave rather similarly to fixed-salinity models throughout the winter growth season, as we and others had observed previously (e.g. Griewank & Notz 2013; Rees Jones & Worster 2014). This study shows that this is a systematic, generic result, not merely an artefact of the particular examples calculated previously. Figure 11 shows that the conclusion holds even for extreme variation in salinity across a wide range of desalination timescales.

However such dynamic-salinity models are still potentially worthwhile for a range of other purposes. There is a direct connection between sea-ice desalination and the buoyancy forcing that drives ocean mixing in the polar oceans. Dynamic-salinity models have a different time dependence of buoyancy forcing relative to fixed-salinity models (Worster & Rees Jones 2015). Furthermore, the brine motion that causes desalination also transports a wide range of biogeochemical tracers and so model differences also affects the evolution of these species (Vancoppenolle *et al.* 2013; Wells, Hitchen & Parkinson 2019). Differences between fixed and dynamic salinity models have been observed both in standalone sea-ice models (Turner & Hunke 2015) and coupled Earth-system models (Bailey *et al.* 2020). Changing the buoyancy forcing can have large-scale effects by changing the amount of dense bottom water being formed (DuVivier *et al.* 2021). Dynamic-salinity models have shown some promise in interpreting data from ice mass balance buoys (Plante *et al.* 2024).

One issue that complicates the comparison of fixed and dynamic models of salinity is the choice of parameters (material properties). While mushy-layer models are formally equivalent to Maykut–Untersteiner/Bitz–Lipscomb models, as shown by Feltham *et al.* (2006), the equivalence relies on an equivalent choice of parameters. In this study, we showed that the default values in CICE/Icepack (Hunke *et al.* 2024a,b) of  $\beta = 0.13 \text{ W m}^{-1} \text{ ppt}^{-1}$  (which controls the sensitivity of thermal conductivity to salinity) is too large to be consistent with mushy-layer theory and would need to be reduced to  $\beta = 0.082 \text{ W m}^{-1} \text{ ppt}^{-1}$  for consistency. While it seems to be well known that the default value of  $\beta$  might be problematic (it is mentioned in the documentation), this inconsistency with mushy-layer theory does not seem well known. Indeed, the recent large-scale studies cited in the previous paragraph have tended to use the ‘bubbly’ model of thermal conductivity from Pringle *et al.* (2007). Schröder *et al.* (2019) showed that this form for the conductivity gave the best agreement with CryoSat-2 observations of sea-ice thickness. When assessing the differences between models, it is important to distinguish structural differences (fixed vs dynamic salinity) from mere parameter choice differences.

Finally, this study proposes an intermediate complexity class of sea-ice model, the QS model. We use a changing coordinate system, transforming the system to a reference frame in which the ice is fixed. We solve a BVP for the temperature field within the ice with no explicit time dependence by including a pseudo-advection term associated with the changing coordinate system. This new term is proportional to the ice growth rate factor. The BVP is then coupled to an IVP for the thickness evolution

of time. This BVP–IVP approach is more complex than the zero-layer Semtner-type model (Semtner 1976) but considerably simpler than full PDE-based models such as Maykut–Untersteiner/Bitz–Lipscomb and their dynamic-salinity successors. The QS model is an exact solution for the initial ice growth when the external forcing is constant, and is used here as a tool to facilitate analytical progress. We also apply it to sinusoidal atmospheric forcing with a range of periods and show that considerable analytical progress can be made in understanding the results (figure 10). Finally, we show that it represents a very good approximation to full PDE-based models even under the most difficult time-dependent atmospheric forcing scenario, a step change (figure 12). This type of intermediate complexity model is likely to be helpful for assessing and understanding the potential impact of any proposed changes to a large-scale model (including, for example, the parameter choices discussed above) as it can be run much more rapidly than a full-PDE model. It may also be valuable in more speculative scenarios such as in modelling potential mushy layers on icy moons (e.g. Buffo *et al.* 2020, 2021; Vance *et al.* 2021) where an idealised modelling approach may allow the parametric uncertainty to be explored thoroughly.

**Acknowledgements.** Insightful comments on an earlier draft by A.J. Wells and M.G. Worster helped improve this manuscript. I also appreciate the comments of two anonymous referees.

**Funding.** This research received no specific grant from any funding agency, commercial or not-for-profit sectors.

**Declaration of interests.** The author reports no conflict of interest.

**Data availability statement.** The code used to generate the results of this study is openly available in on the Zenodo repository at <https://zenodo.org/doi/10.5281/zenodo.13710756> (Rees Jones 2024).

**Author ORCID.**

 David W. Rees Jones <https://orcid.org/0000-0001-8698-401X>.

## Appendix A. Estimation of the relative importance of additional terms in heat equation relating to brine transport and desalination

The heat equation derived in mushy-layer models of sea ice has additional terms relating to the evolution of bulk salinity that are not present in the heat equation (2.8) used in this study. In particular, a more general version of this equation is

$$c \frac{\partial T}{\partial t} + \tilde{c} w \frac{\partial T}{\partial z} = \kappa_s \frac{\partial}{\partial z} \left( k \frac{\partial T}{\partial z} \right), \quad (\text{A1})$$

where  $w$  is the vertical brine velocity and

$$\tilde{c} = \frac{c_l}{c_s} + \frac{L}{c_s(-T)}. \quad (\text{A2})$$

The first term in  $\tilde{c}$  arises from brine advection, i.e. the heat transported by the motion of brine through the porous matrix of sea ice. The second term in  $\tilde{c}$  arises from the desalination of the ice, which causes a reduction in liquid fraction and hence a source of latent heat. A full derivation is given in Feltham *et al.* (2006) and Rees Jones & Worster (2014), for example.

The ratio of the second to the first term in  $\tilde{c}$  is  $L/c_l(-T)$ . But  $L/c_l \approx 77^\circ\text{C}$  (§ 2.4) and  $-T$  is between about  $2^\circ\text{C}$  and  $20^\circ\text{C}$ , so this ratio is much greater than 1. Physically, the heat directly transported by brine advection is always negligible compared with the contribution from latent heating.

Equation (A1) does not determine the brine velocity  $w$ . In general, it will be determined by convective desalination and flushing. Determining  $w$  has been one of the areas of recent development in sea-ice modelling, as discussed in § 1.

To estimate the order of magnitude significance of the extra term in (A1), we instead use the conservation equation for bulk salinity

$$\frac{\partial S}{\partial t} + w \frac{\partial C}{\partial z} = 0, \quad (\text{A3})$$

where we have neglected diffusion of salt (e.g. Feltham *et al.* 2006; Rees Jones & Worster 2014). Indeed, Wells *et al.* (2019) showed that salt diffusion had a relatively modest effect on the growth of sea ice. But  $C$  is linearly related to  $T$  through equation (2.5), so

$$w \frac{\partial T}{\partial z} = -mw \frac{\partial C}{\partial z} = m \frac{\partial S}{\partial t}. \quad (\text{A4})$$

Then equation (A1) can be rewritten

$$c \frac{\partial T}{\partial t} + \tilde{c} m \frac{\partial S}{\partial t} = \kappa_s \frac{\partial}{\partial z} \left( k \frac{\partial T}{\partial z} \right). \quad (\text{A5})$$

Thus, if the ice salinity is constant (as we assumed throughout our calculations except in § 5.2), then the term involving  $\tilde{c}$  is zero.

For variable salinity (§ 5.2), if we assume that time scale for salinity change  $\Delta S$  occurs at a comparable rate to that of temperature  $\Delta T$ , then the ratio of the second to the first term on the left-hand side of (A5) can be estimated

$$\frac{\tilde{c} m \partial S / \partial t}{c \partial T / \partial t} \sim \frac{\tilde{c} m \Delta S}{c \Delta T} \sim \frac{\Delta S (-T)}{S \Delta T}. \quad (\text{A6})$$

In deriving this estimate, we assumed that both  $\tilde{c}$  and  $c$  are dominated by the terms involving latent heat for the reasons discussed above. Both fractions at the end of (A6) are, in general,  $O(1)$ , so we would expect both terms on the left-hand side of (A5) to matter. However, within the QS framework (§ 2.7), we map evolution in time into  $(\tau, \zeta)$  coordinates and neglect any explicit dependence on  $\tau$ . Therefore, if salinity is taken as constant or a function of  $\tau$  only, it is self-consistent to neglect the term involving  $\tilde{c}$ , as we have done in the main body of this study. The most complex  $\tau$ -dependent salinity variation considered is found in § 5.2, elsewhere the salinity is constant. For a more general salinity evolution, both terms are, in principle, the same order of magnitude. To reiterate, the dominant contribution from desalination comes from latent heat release, not brine advection directly.

## Appendix B. Asymptotic solution of BVP for initial growth rate factor $q_0$

Here, we provide a more detailed derivation of the asymptotic estimates given in § 3.2. Under the assumptions stated in the main text ( $\theta_e = 0$ ,  $\Delta c = 0$ ,  $\hat{L}^{-1} \rightarrow 0$ ), the full BVP

(3.1) can be written

$$-\frac{c}{\hat{L}}\zeta q_0\theta' = (k\theta')', \quad \theta(0) = 0, \quad \theta(1) = 1, \quad q_0 = \frac{(k\theta')(1)}{1 - \hat{S}}, \quad (\text{B1a-d})$$

where the material properties are taken from (2.22),

$$X = \hat{S} \frac{\theta_B - 1}{\theta_B - \theta}, \quad k = 1 - X\Delta k, \quad \frac{c}{\hat{L}} = \frac{1}{\theta_B - \theta} X. \quad (\text{B2a-c})$$

Note that the limit  $\hat{L}^{-1} \rightarrow 0$  justifies the loss of two terms in the simplified expression for  $c/\hat{L}$  given here, although  $c/\hat{L}$  itself must be retained.

We then make the ansatz

$$\theta \sim \zeta + \hat{S}\tilde{\theta}(\zeta) + O(\hat{S}^2), \quad (\text{B3})$$

and substitute this expression into the BVP. Note that  $c/\hat{L} \propto X = O(\hat{S})$ , so we can need only consider the leading order temperature profile ( $\theta \sim \zeta$ ) and leading order estimate of the growth rate factor ( $q_0 \sim 1$ ) on the left-hand side of (B1a). We obtain

$$-\hat{S} \frac{\theta_B - 1}{(\theta_B - \zeta)^2} \zeta = \left[ \left( 1 - \Delta k \hat{S} \frac{\theta_B - 1}{\theta_B - \zeta} \right) (1 + \hat{S}\tilde{\theta}') \right]' + O(\hat{S}^2). \quad (\text{B4})$$

By equating terms at  $O(\hat{S})$ , and after some algebraic manipulation, we obtain

$$\tilde{\theta}'' = \frac{\theta_B - 1}{(\theta_B - \zeta)^2} (\Delta k - \zeta). \quad (\text{B5})$$

We integrate once to obtain

$$\frac{\tilde{\theta}'}{\theta_B - 1} = \frac{\Delta k - \theta_B}{\theta_B - 1} - \log(\theta_B - \zeta) + C, \quad (\text{B6})$$

where  $C$  is constant. We integrate again to obtain

$$\frac{\tilde{\theta}}{\theta_B - 1} = (2\theta_B - \Delta k - \zeta) \log(\theta_B - \zeta) + (1 + C)\zeta + D, \quad (\text{B7})$$

where  $D$  is constant. Here  $D$  is determined by the boundary condition (B1b):

$$D = -(2\theta_B - \Delta k) \log(\theta_B). \quad (\text{B8})$$

Then  $C$  is determined by the boundary condition (B1c):

$$C = -(2\theta_B - \Delta k - 1) \log(\theta_B - 1) - 1 + (2\theta_B - \Delta k) \log(\theta_B). \quad (\text{B9})$$

To calculate the (extra contribution to the) temperature gradient at the ice–ocean interface, we substitute (B9) into (B6) at evaluate at  $\zeta = 1$  and obtain, after simplification,

$$\tilde{\theta}'(1) = 1 + \Delta k - 2\theta_B - (\theta_B - 1)(2\theta_B - \Delta k) \log(1 - \theta_B^{-1}). \quad (\text{B10})$$

Finally, by expanding the final boundary condition (B1d),

$$q_0 \sim 1 + \hat{S}[1 - \Delta k + \tilde{\theta}'(1)] + O(\hat{S}^2), \quad (\text{B11})$$

and combining with (B10), we obtain the result

$$q_0 \sim 1 + \hat{S}(\theta_B - 1) \left[ -2 - (2\theta_B - \Delta k) \log(1 - \theta_B^{-1}) \right] + O(\hat{S}^2). \quad (\text{B12})$$

This result is reported as (3.7) in the main text where we present numerical evidence (figure 4) that this asymptotic limit holds well even up to moderate values of  $\hat{S}$ .



## REFERENCES

- ANDERSON, D.M. & GUBA, P. 2020 Convective phenomena in mushy layers. *Annu. Rev. Fluid Mech.* **52**, 93–119.
- BAILEY, D.A., HOLLAND, M.M., DUVIVIER, A.K., HUNKE, E.C. & TURNER, A.K. 2020 Impact of a new sea ice thermodynamic formulation in the CESM2 sea ice component. *J. Adv. Model Earth Syst.* **12** (11), e2020MS002154.
- BITZ, C.M. & LIPSCOMB, W.H. 1999 An energy-conserving thermodynamic model of sea ice. *J. Geophys. Res.* **104** (C7), 15669–15677.
- BUFFO, J.J., SCHMIDT, B.E., HUBER, C. & MEYER, C.R. 2021 Characterizing the ice-ocean interface of icy worlds: a theoretical approach. *Icarus* **360**, 114318.
- BUFFO, J.J., SCHMIDT, B.E., HUBER, C. & WALKER, C.C. 2020 Entrainment and dynamics of ocean-derived impurities within Europa's ice shell. *J. Geophys. Res.* **125** (10), e2020JE006394.
- DING, G.-Y., WELLS, A.J. & ZHONG, J.-Q. 2019 Solidification of binary aqueous solutions under periodic cooling. Part 1. Dynamics of mushy-layer growth. *J. Fluid Mech.* **870**, 121–146.
- DUVIVIER, A.K., HOLLAND, M.M., LANDRUM, L., SINGH, H.A., BAILEY, D.A. & MAROON, E.A. 2021 Impacts of sea ice mushy thermodynamics in the Antarctic on the coupled Earth system. *Geophys. Res. Lett.* **48** (18), e2021GL094287.
- FELTHAM, D.L., UNTERSTEINER, N., WETTLAUER, J.S. & WORSTER, M.G. 2006 Sea ice is a mushy layer. *Geophys. Res. Lett.* **33**, L14501.
- GOLDEN, K.M., *et al.* 2020 Modeling sea ice. *Not. Am. Math. Soc.* **67** (10), 1535–1555.
- GRIEWANK, P.J. & NOTZ, D. 2013 Insights into brine dynamics and sea ice desalination from a 1-D model study of gravity drainage. *J. Geophys. Res.* **118** (7), 3370–3386.
- GRIEWANK, P.J. & NOTZ, D. 2015 A 1-D modelling study of Arctic sea-ice salinity. *Cryosphere* **9** (1), 305–329.
- HITCHEN, J. & WELLS, A.J. 2016 The impact of imperfect heat transfer on the convective instability of a thermal boundary layer in a porous media. *J. Fluid Mech.* **794**, 154–174.
- HUNKE, E.C., *et al.* 2024a CICE-Consortium/CICE: CICE Version 6.5.1. <https://doi.org/10.5281/zenodo.11223920>.
- HUNKE, E.C., *et al.* 2024b CICE-Consortium/Icepack: Icepack 1.4.1. <https://doi.org/10.5281/zenodo.11223808>.
- HUPPERT, H.E. & WORSTER, M.G. 1985 Dynamic solidification of a binary melt. *Nature* **314** (6013), 703–707.
- KEEN, A., *et al.* 2021 An inter-comparison of the mass budget of the Arctic sea ice in CMIP6 models. *Cryosphere* **15** (2), 951–982.
- KERR, R.C., WOODS, A.W., WORSTER, M.G. & HUPPERT, H.E. 1989 Disequilibrium and macrosegregation during solidification of a binary melt. *Nature* **340** (6232), 357–362.
- KERR, R.C., WOODS, A.W., WORSTER, M.G. & HUPPERT, H.E. 1990 Solidification of an alloy cooled from above. Part 1. Equilibrium growth. *J. Fluid Mech.* **216**, 323–342.
- KIERZENKA, J. & SHAMPINE, L.F. 2001 A BVP solver based on residual control and the MATLAB PSE. *ACM Trans. Math. Softw.* **27** (3), 299–316.
- MAYKUT, G.A. & UNTERSTEINER, N. 1969 *Numerical Prediction of the Thermodynamic Response of Arctic Sea Ice to Environmental Changes*. RAND Corporation.
- MAYKUT, G.A. & UNTERSTEINER, N. 1971 Some results from a time-dependent thermodynamic model of sea ice. *J. Geophys. Res.* **76** (6), 1550–1575.
- NOTZ, D. 2005 Thermodynamic and fluid-dynamical processes in sea ice. PhD thesis, University of Cambridge, Cambridge.
- NOTZ, D. & WORSTER, M.G. 2008 In situ measurements of the evolution of young sea ice. *J. Geophys. Res.* **113**, C03001.
- PLANTE, M., LEMIEUX, J.-F., TREMBLAY, L.B., TIVY, A., ANGNATOK, J., ROY, F., SMITH, G., DUPONT, F. & TURNER, A.K. 2024 Using Icepack to reproduce ice mass balance buoy observations in landfast ice: improvements from the mushy-layer thermodynamics. *Cryosphere* **18** (4), 1685–1708.
- PRINGLE, D.J., EICKEN, H., TRODAHL, H.J. & BACKSTROM, L.G.E. 2007 Thermal conductivity of landfast Antarctic and Arctic sea ice. *J. Geophys. Res.* **112**, C04017.
- REES JONES, D.W. 2024 Sea-ice-similarity software. <https://doi.org/10.5281/zenodo.13710756>.
- REES JONES, D.W. & WORSTER, M.G. 2013a Fluxes through steady chimneys in a mushy layer during binary alloy solidification. *J. Fluid Mech.* **714**, 127–151.
- REES JONES, D.W. & WORSTER, M.G. 2013b A simple dynamical model for gravity drainage of brine from growing sea ice. *Geophys. Res. Lett.* **40** (2), 307–311.

- REES JONES, D.W. & WORSTER, M.G. 2014 A physically based parameterization of gravity drainage for sea-ice modeling. *J. Geophys. Res.* **119** (9), 5599–5621.
- ŠARLER, B. & ŽIDAR 1995 Stefan's work on solid–liquid phase changes. *Engng Anal. Bound. Elem.* **16** (2), 83–92.
- SCHRÖDER, D., FELTHAM, D.L., TSAMADOS, M., RIDOUT, A. & TILLING, R. 2019 New insight from CryoSat-2 sea ice thickness for sea ice modelling. *Cryosphere* **13** (1), 125–139.
- SEMTNER, A.J. 1976 A model for the thermodynamic growth of sea ice in numerical investigations of climate. *J. Phys. Oceanogr.* **6** (3), 379–389.
- STEFAN, J. 1891 Über die theorie der eisbildung, insbesondere über die eisbildung im polarmeere. *Ann. Phys.* **278** (2), 269–286.
- THOMAS, M., VANCOPPENOLLE, M., FRANCE, J.L., STURGES, W.T., BAKKER, D.C.E., KAISER, J. & VON GLASOW, R. 2020 Tracer measurements in growing sea ice support convective gravity drainage parameterizations. *J. Geophys. Res.* **125** (2), e2019JC015791.
- TURNER, A.K. & HUNKE, E.C. 2015 Impacts of a mushy-layer thermodynamic approach in global sea-ice simulations using the CICE sea-ice model. *J. Geophys. Res.* **120** (2), 1253–1275.
- TURNER, A.K., HUNKE, E.C. & BITZ, C.M. 2013 Two modes of sea-ice gravity drainage: a parameterization for large-scale modeling. *J. Geophys. Res.* **118** (5), 2279–2294.
- VANCE, S.D., JOURNAUX, B., HESSE, M. & STEINBRÜGGE, G. 2021 The salty secrets of icy ocean worlds. *J. Geophys. Res.* **126** (1), e2020JE006736.
- VANCOPPENOLLE, M., *et al.* 2013 Role of sea ice in global biogeochemical cycles: emerging views and challenges. *Quat. Sci. Rev.* **79**, 207–230.
- VANCOPPENOLLE, M., FICHEFET, T. & BITZ, C.M. 2005 On the sensitivity of undeformed Arctic sea ice to its vertical salinity profile. *Geophys. Res. Lett.* **32**, L16502.
- VANCOPPENOLLE, M., FICHEFET, T., GOOSSE, H., BOUILLON, S., MADEC, G. & MORALES MAQUEDA, M.A. 2009 Simulating the mass balance and salinity of Arctic and Antarctic sea ice. 1. Model description and validation. *Ocean Model.* **27** (1), 33–53.
- VUIK, C. 1993 Some historical notes about the Stefan problem. *Tech. Rep.* 93–07. Reports of the Faculty of Technical Mathematics and Informatics, Delft University of Technology.
- WELLS, A.J., HITCHEN, J.R. & PARKINSON, J.R.G. 2019 Mushy-layer growth and convection, with application to sea ice. *Phil. Trans. R. Soc. A* **377** (2146), 20180165.
- WELLS, A.J., WETTLAUFER, J.S. & ORSZAG, S.A. 2011 Brine fluxes from growing sea ice. *Geophys. Res. Lett.* **38**, L04501.
- WELLS, A.J., WETTLAUFER, J.S. & ORSZAG, S.A. 2013 Nonlinear mushy-layer convection with chimneys: stability and optimal solute fluxes. *J. Fluid Mech.* **716**, 203–227.
- WETTLAUFER, J.S. 1991 Heat flux at the ice-ocean interface. *J. Geophys. Res.* **96** (C4), 7215–7236.
- WETTLAUFER, J.S., WORSTER, M.G. & HUPPERT, H.E. 1997 Natural convection during solidification of an alloy from above with application to the evolution of sea ice. *J. Fluid Mech.* **344**, 291–316.
- WORSTER, M.G. 1986 Solidification of an alloy from a cooled boundary. *J. Fluid Mech.* **167**, 481–501.
- WORSTER, M.G. 1997 Convection in mushy layers. *Annu. Rev. Fluid Mech.* **29** (1), 91–122.
- WORSTER, M.G. 2000 Solidification of fluids. In *Perspectives in Fluid Dynamics: A Collective Introduction to Current Research* (ed. G.K. Batchelor, H.K. Moffatt & M.G. Worster), pp. 393–446. Cambridge University Press.
- WORSTER, M.G. & REES JONES, D.W. 2015 Sea-ice thermodynamics and brine drainage. *Phil. Trans. R. Soc. A* **373** (2045), 20140166.